remote sensing

MDPI

Review

The Arctic Amplification and Its Impact: A Synthesis Through Satellite Observations

Igor Esau[1,2,*], Lasse H. Pettersson[1], Mathilde Cancet[3], Bertrand Chapron[4], Alexander Chernokulsky[5], Craig Donlon[6], Oleg Sizov[7], Andrei Soromotin[8] and Johnny A. Johannesen[1]

[1] Nansen Environmental and Remote Sensing Center, Jahnebakken 3, 5007, Bergen, Norway; lasse.pettersson@nersc.no (L.H.P); johnny.johannessen@nersc.no (J.A.J)
[2] UiT – The Arctic University of Norway, Dept. of Physics and Technology, 9037, Tromsø, Norway;
[3] NOVELTIS, Labège, 31670, France; mathilde.cancet@noveltis.fr
[4] Ifremer, 1625 Rte de Sainte-Anne, 29280 Plouzané, France; bchapron@ifremer.fr
[5] A.M. Obukhov Institute of Atmospheric Physics of the Russian Academy of Science, 3 Pyzhevsky, 119017 Moscow, Russia , Russia; a.chernokulsky@ifaran.ru
[6] Earth Surfaces and Interior Section (EOP-SME), Earth and Mission Science Division, European Space Agency/ESTEC, Keplerlaan 1, 2201 AZ, Noordwijk, The Netherlands; craig.donlon@esa.int
[7] Oil and Gas Research Institute of the Russian Academy of Sciences (OGRI RAS), 3 Gubkina St., Moscow, Russia, 119333; kabanin@yandex.ru
[8] Institute of Ecology and Natural Resources Management, Tyumen State University, Volodarskogo, 6, Tyumen, 625003, Russia; asoromotin@mail.ru
* Correspondence: igor.ezau@uit.no

Citation: Esau, I.; Pettersson, L.H.; Cancet, M.; Chapron, B.; Chernokulsky, A.; Donlon, C.; Sizov, O.; Soromotin, A.; Johannesen, J.A. The Arctic amplification and its impact: A synthesis through satellite observations. 2023, *14*, x. https://doi.org/10.3390/xxxxx

Academic Editor(s): Joan Masó; Ivette Serral; Alaitz Zabala Torres

Received: 09 January 2023
Accepted: 25 February 2023
Published: date

Publisher's Note: MDPI stays neutral with regard to jurisdictional claims in published maps and institutional affiliations.

Abstract: Arctic climate change has already resulted in amplified and accelerated regional warming, or the Arctic amplification. Satellite observations have captured this climate phenomenon in its development and in sufficient spatial details. As such, these observations have been—and still are—indispensable for monitoring of the amplification in this remote and inhospitable region, which is sparsely covered with ground observations. This study synthesizes the key contributions of satellite observations into an understanding and characterization of the amplification. The study reveals that the satellites were able to capture a number of important environmental transitions in the region that both precede and follow the emergence of the apparent amplification. Among those transitions, we find a rapid decline in the multiyear sea ice and subsequent changes in the surface radiation balance. Satellites have witnessed the impact of the amplification on phytoplankton and vegetation productivity as well as on human activity and infrastructure. Satellite missions of the European Space Agency (ESA) are increasingly contributing to amplification monitoring and assessment. The ESA Climate Change Initiative has become an essential provider of long-term climatic-quality remote-sensing data products for essential climate variables. Still, such synthesis has found that additional efforts are needed to improve cross-sensor calibrations and retrieval algorithms and to reduce uncertainties. As the amplification is set to continue into the 21st century, a new generation of satellite instruments with improved revisiting time and spectral and spatial resolutions are in high demand in both research and stakeholders' communities.

Keywords: European Space Agency; Climate Change Initiative; Arctic amplification; satellite observations; climate change monitoring

1. Introduction

On May 29th, 2020, a power plant oil reservoir near Norilsk, Russia collapsed, causing one of the largest oil spills and incidences of extensive land and water contamination in the Arctic. About 17,000 tons of diesel went into the river Ambarnaya and streamed down towards the large lake Pyasino (see Figure 1). Nobody was injured in this remote area, but the total cost of the disaster exceeded USD 2 billion. This accident became a rallying cry, among other such unpleasant reminders, of rapid Arctic warming and its adverse impact on the natural environment, infrastructure, and society in the region. Moreover, the accident highlighted the indispensable role of satellite observations' disclosure of the true scale and extent of damages. The European Space Agency (ESA)'s Sentinel-2 platform has been used to complement the analysis, field photographs, and historical data covering the 1980–2020 daily air temperature and precipitation, permafrost observations, and modeling—all diverse materials that helped to attribute this accident to the Arctic amplification of global warming [1]. Its immediate cause, a collapsing pillar, was accidental and local. Yet this collapse occurred due to more persistent and large-scale climate factors, namely, accelerated permafrost thaw that followed the abnormally warm weather in May 2020. The permafrost thaw and weakened ground-bearing capacities were the result of preceding decades of climate change [2].

Figure 1. The Copernicus Sentinel-2 image of an oil (diesel) spill into the river Ambarnaya near Norilsk, Russia. The image, from 1 June 2020, was processed by the ESA and has been made available under CC BY-SA 3.0 IGO license at https://www.esa.int/ESA_Multimedia/Images/2020/06/Arctic_Circle_oil_spill.

Capturing the climate change over a relatively short period—the majority of remote-sensing data products have become available since 1979 [3]—satellite observations have proven to be crucial for the discovery and monitoring of important changes in the earth's climate system [4]. Particularly, Arctic climate studies and environmental monitoring have benefited from the high density of cross sections of polar-orbiting satellites [5]. Arguably, many climate phenomena would not have been detected by climate models and conventional observations alone [4], for example, the spatial pattern of sea ice retreat [6] and increasing biological productivity (greening) in the high northern latitudes [7]. One such impactful phenomenon is a climatic transition from multiyear to seasonal sea ice in the Arctic Ocean [8], which unlocked surface feedback leading to the emergence of the apparent amplification in the 21st century [9].

The longest time series (since 1966) of satellite observations exists for snow cover [10]. Figure 2 presents the temporal coverage for essential climate variables (ECVs) collected in the ESA Climate Change Initiative (CCI). The ESA CCI efforts are central for synthesis; ECVs are considered from the perspective of physical climatology of the Arctic amplification. ECVs provide reliable, traceable, observation-based evidence for a range of climate applications, including monitoring and attributing of climate change phenomena [11]. The ECV concept has been adopted by space agencies operating Earth observation satellites. At present, ESA CCI comprises 23 parallel ECV projects, a dedicated climate-modeling project for the assessment of products, a portal (https://climate.esa.int/en/odp/#/dashboard) providing the products, a toolbox to facilitate the combining and analysis of the products, and a visualization tool supporting outreach. Although climatic-quality ECV records require data fusion from many space-born sensors and missions, the ESA satellite missions were of critical importance for many ECVs. A timeline of all ESA satellite missions can be found in the online Earth Observation Handbook, in the CEOS database at http://database.eohandbook.com/measurements/overview.aspx (last visited 26.11.2022). Starkweather et al. [12] provided a wider perspective on a value chain for the Arctic Observing Network that combines both satellite and ground-based (in situ) monitoring systems. The value chain traces the impact of satellite observations (in combination with other data sets and models) down to vital signs of climate change and societal impact.

Polar-orbiting satellites have captured details of the major environmental transitions in the Arctic with a variety of space-born instruments. This has helped in the development of robust long-term ECV records, trend analysis, and the study of the amplification [13].

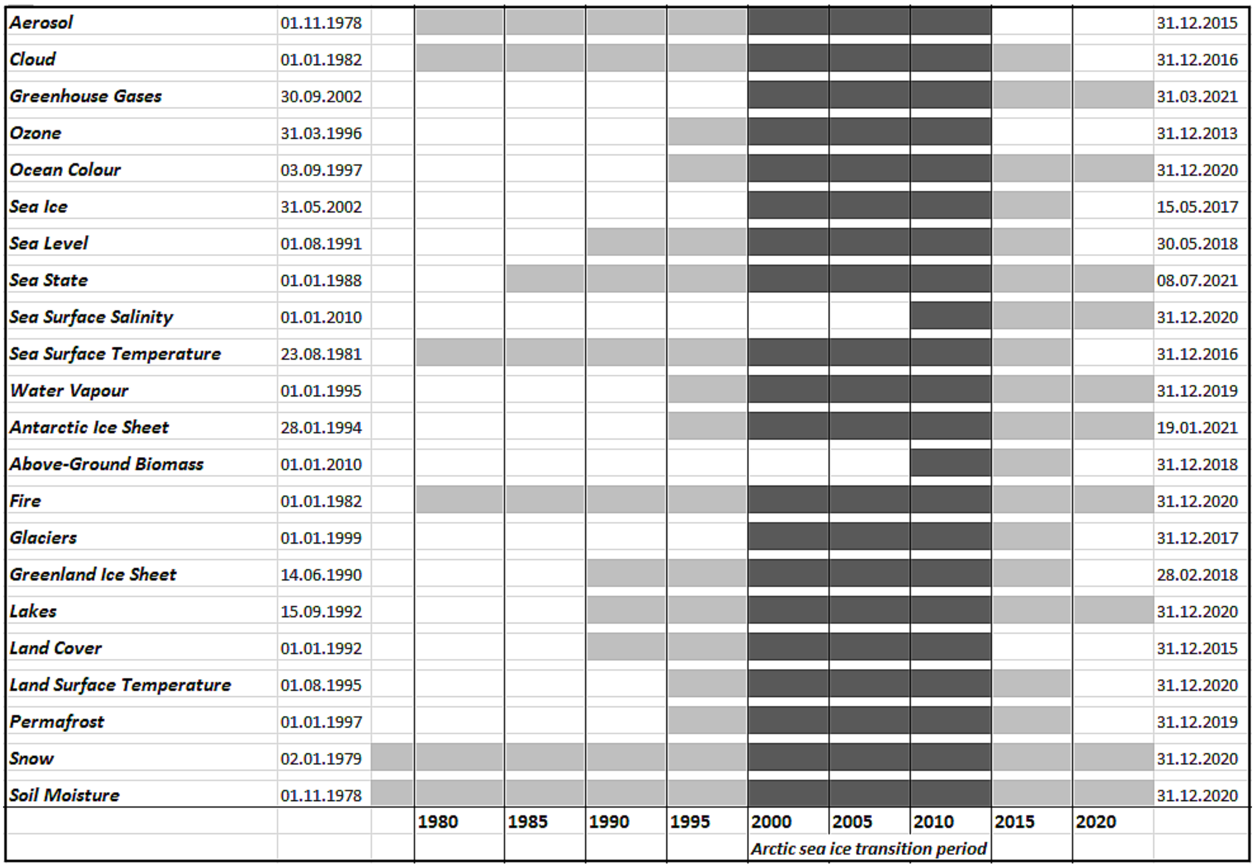

Figure 2. Temporal coverage of climate data records for ECVs in the ESA CCI. Dates and filled bars indicate availability of the data sets in the ESA CCI portal (https://climate.esa.int/) by the end of 2022. Dark shading indicates the period of apparent amplification emergence.

This study is a synthesis of the satellite contribution to the assessment of the Arctic amplification, which we will refer to as just the amplification. The amplification is defined as an accelerated and amplified regional climate change; it is primarily atmospheric and surface warming, but it is also related to a diverse set of influential climate phenomena [14,15]. We schematically illustrate the most important phenomena and their links to satellite observations in Figure 3. The paper is organized as follows. Section 2 presents the relevant literature, data, and methods. Section 3 is focused on the synthesis and discussion of the satellite contributions into the understanding of the amplification. Section 4 outlines the broader impact of the amplification identified through satellite observations. Section 5 highlights the conclusions and recommendations of this study. It should be emphasized that we do not follow an unfortunate but popular trend of composing a meta-analysis solely on the basis of automatically relevant literature. On the contrary, this synthesis is guided by a new amplification paradigm that has crystallized in modeling studies (e.g., Previdi et al., 2021; Semenov, 2021). The focus on satellite observations makes our work complementary to the recent comprehensive reviews by Taylor et al. [9] and Wendisch et al. [16], which synthesize modeling results. At the same time, this synthesis is distinct from the recent comprehensive reviews of satellite observations by Duncan et al. [5] and earlier reviews by Comiso and Hall [13] and Wang et al. [17]. We consider satellite observations from the perspective of physical climatology.

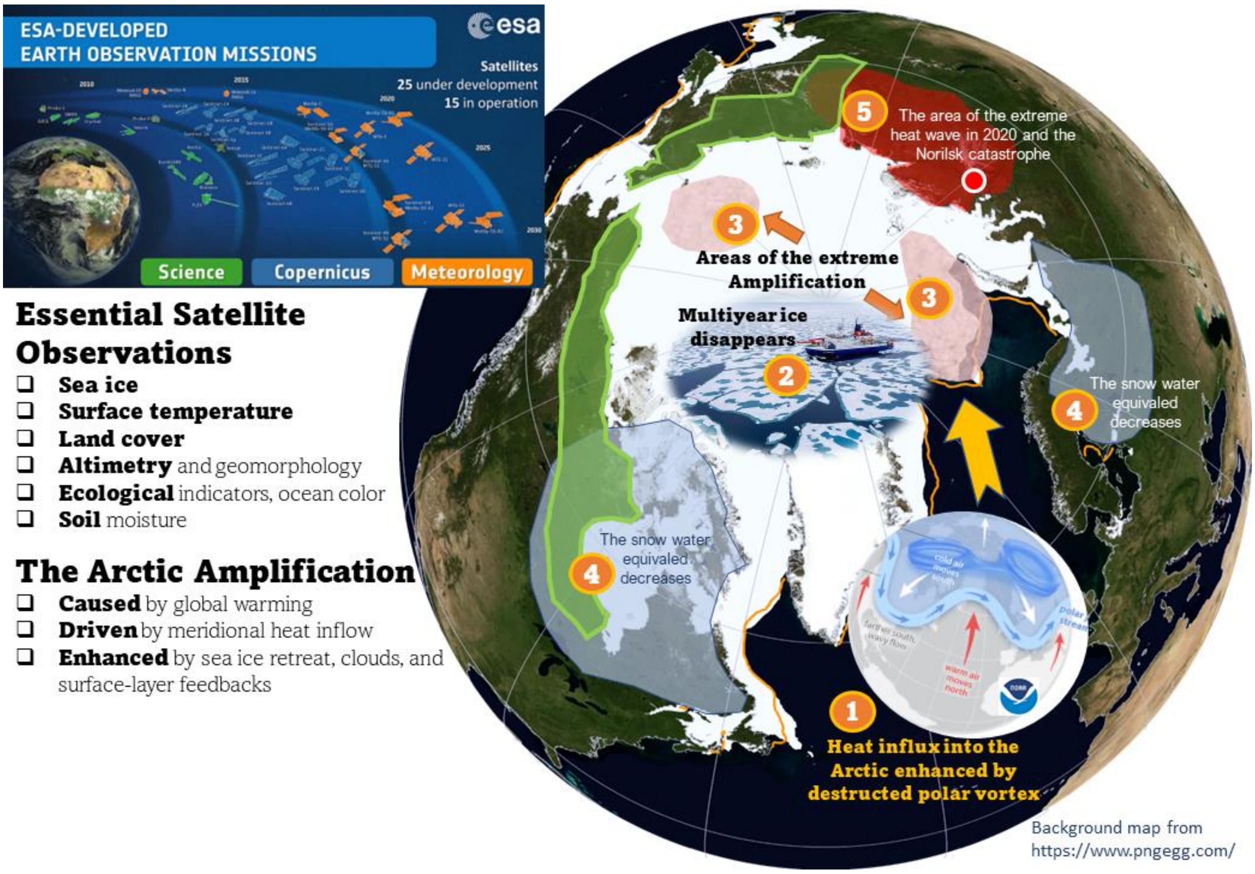

Figure 3. A schematic illustration of the ESA satellite fleet contributing to monitoring of the dynamic processes, physical feedback, and environmental impact related to the emergence of the apparent amplification.

2. Definition, Literature, Data, and Methods

Definition. Anthropogenic climate change is global. However, surface warming is uneven in space and time; the Arctic has experienced the regional amplification of this warming over the last three to five decades [18]. Moreover, the amplification in some limited Arctic areas, such as the northern Barents-Kara sea region, is exceptional and has no parallels elsewhere [19]. Although the amplification is an intuitive concept, it is not so unambiguous. Here, we rely on the amplification metrics found in recent studies [20–22]. The amplification can be defined through the difference, Δ_{AA}, and the ratio, R_{AA}, of air temperature changes in the Arctic, ΔT_A, and over the northern hemisphere (0-90°N) or the northern extra-tropics (20-60°N), ΔT_H:

$$\Delta_{AA} = \Delta T_A - \Delta T_H, \tag{1}$$

$$R_{AA} = \frac{\Delta T_A}{\Delta T_H}. \tag{2}$$

The Arctic is typically defined as the region to the north of 60°N, 65°N, or 70°N (in this case, covering mostly the Arctic Ocean). Different definitions result in different values—the more limited the area of the Arctic is considered, the larger amplification indices are found [19,22]—but trends and variability of the phenomena are not significantly different. This similarity clearly indicates that the amplification patterns are localized in the high Arctic latitudes.

The amplification metrics are imperfect. A short-term trend of Δ_{AA}, i.e., $\frac{d\Delta_{AA}}{dt}$, would be a more justified measure of the regional temperature trends' divergence. This is, however, highly ambiguous against the backdrop of high Arctic climate variability, and it is hence used infrequently. A strong amplification ($R_{AA} \gg 1$) will be found during periods of transitional climate change, whereas approaching an equilibrium climate state will lead to $R_{AA} \approx 1$. Such behavior can be misleading. The averaging and aggregation of anomalies over longer periods (e.g., over 30 years) have been proposed to improve the statistical stability of the metrics [18,21,23]. As we will show, a longer averaging and aggregation impedes the identification of important physical transitions in the Arctic climate system that have a decisive impact on the amplification.

Literature. We are primarily interested in reviews and the synthesis of publications dealing with consistent long-term (climatic) satellite observations of temperature and closely related ECVs. We recommend the comprehensive review of Duncan et al. [5] to the reader interested in specific contributions from concrete instruments and satellite platforms. A detailed review of satellite temperature observations can be found in Comiso and Hall [13]. More recently, sea and ice surface temperatures from satellites (review and data sets) were published in [24]. A review of sea ice characteristics was published by Wang et al. [17]; a review of snow cover trends is found in Bormann et al. [25]; a review of phytoplankton dynamics is available in Ardyna and Arrigo [26]. Products and methods for monitoring changes in more complicated environmental indicators such as terrestrial vegetation cover [7] and permafrost [27] have also received considerable attention [28,29]. Several reviews have also attempted a holistic assessment of the Arctic environmental changes on the basis of satellite data products [30]. Data products covering two, three, and four decades of climate change combine data sets from successive satellite platforms/missions bearing similar instruments [28]. Table 1 lists some key recent reviews with a focus on satellite observations of Arctic climate change.

Table 1. List of key recent reviews focusing on satellite observations of Arctic climate change.

Reference	Key Notes and Brief Conclusions
	General reviews
[4]	Satellite observations are indispensable for climate monitoring.
[5]	Satellites plays a vital role in Arctic climate change assessment.
[31]	Satellites reveal climate change footprints in the Arctic energy budget.
[32]	Satellites reveal changes in the radiation balance.
[33] [13]	Satellites disclose the amplified Arctic warming.
[9]	Satellites reveal interconnections in the amplification drivers, feedback, and geographical patterns.
[19] [34] [35]	Exceptional warming over Barents Sea is related to sea ice retreat and declining sea ice import.
	Specific reviews

	Dynamical factors of the amplification
[36]	Increase in ocean warm water inflow
[37]	Decrease in meridional heat transport since 2000
[38]	Decrease in middle atmosphere temperature inversion strength
	Local factors and feedback of the amplification
[39] [40]	Increase in land surface temperatures with minimum trends in summer and maximum trends in autumn; atmospheric temperature inversions correlated with sea ice anomalies
[6] [24]	Rise in Arctic sea surface temperatures
[41] [19]	Surface air and sea surface temperatures correlated with sea ice cover
[17] [42] [43] [44]	Satellites show disappearance of multiyear ice and reduction in ice thickness and volume
[45]	Increase in area of melting ponds on ice
[25] [46]	General decrease in extent of snow cover and water equivalent, but geographical variations are significant
[47]	Arctic cloud cover undergoes multidirectional changes
[48]	Regional changes in TOA radiation fluxes are insignificant—implies weak atmosphere–surface coupling
[49] [50] [51]	Decrease in Arctic ice surface albedo
[52]	Increase in sea ice radiative forcing
[53]	Increase in cloud radiative forcing
	Environmental changes
[30]	Satellite observations reveal rapid changes in the Arctic environment; list of relevant satellite data sets provided
[7] [28]	Satellite observations reveal complex changes in the Arctic environment
[54] [55] [29] [56] [27]	Satellite observations could be used to monitor permafrost thaw; permafrost becoming unstable in different regions
[57]	Growing season duration and increase in productivity of vegetation
[26]	Satellites reveal increasing marine biological production in the Arctic
[58,59] [60]	Loss in Greenland ice sheet mass and height
	Impact on humans
[61] [62]	Satellites reveal expanding human infrastructure and growing impact in the Arctic

Three prominent examples highlight the significance of satellite observations for amplification studies. One example is given by the Greenland ice sheet studies. An unprecedented loss of Greenland ice (100 to 255 Gt of ice per year) has been inferred from a synthetic data product for ice mass balance (elevation) monitoring [63]. The first data were collected in the late 1970s by the National Aeronautics and Space Administration (NASA)'s Geodetic and Earth Orbiting Satellite-3 (GEOS-3), NASA's Seasat, and the US

Navy's Geosat oceanographic radar altimeters. These data were combined with observations from a fleet of missions that provided for different products, e.g., GRACE and GRACE-FO [60]. Another example is given by the University of Alabama in Huntsville (UAH)'s Microwave Sounding Unit (MSU) and Advanced Microwave Sounding Unit (AMSU) product that records the temperature of upper atmosphere data [64,65]. It combines data from NOAA satellite series and data from the TIROS-N (1978-1979), Aqua (2002-2009), and MetOP A (2007–2016) and B (2012-2016) satellites, which do not bear identical instrumentation. Yet another example refers to the Global Inventory Modeling and Mapping Studies Normalized Difference Vegetation Index data set (GIMMS3g), which is widely used to assess long-term vegetation changes [66].

The ESA Copernicus Sentinel missions have opened a new era of polar satellite observations. The missions consist of a family of satellites designed for the operational monitoring of the Earth system with continuity up to 2030 and beyond. On-board sensors include both radar and multi-spectral imagers for land, ocean, sea ice, snow cover, ice sheets, glaciers, and atmospheric monitoring. Sentinel-1 is a polar-orbiting, all-weather, day-and-night radar imaging mission for land and ocean services. Sentinel-1A was launched on 3 April 2014, and Sentinel-1B on 25 April 2016. Sentinel-2 is a polar-orbiting, multi-spectral high-resolution imaging mission for land monitoring. Sentinel-2A was launched on 23 June 2015, and Sentinel-2B followed on 7 March 2017. Sentinel-3 is a polar-orbiting multi-instrument mission to measure sea surface topography, sea and land surface temperature, ocean color, and land color with high-end accuracy and reliability. Sentinel-3A was launched on 16 February 2016, and Sentinel-3B on 25 April 2018. Sentinel-5 is a polar-orbiting instrument aboard a MetOp Second Generation satellite with a focus on air quality and climate. Sentinel-5P has been orbiting since 13 October 2017. Sentinel-6 is a polar-orbiting mission carrying a radar altimeter to measure global sea surface heights, primarily for operational oceanography and for climate studies. The European earth's observation teams have identified several gaps and needs in the satellite monitoring of the polar regions. The most important characteristics are related to latency time and a lower revisit time [67]. Reductions in the revisit time to 3 h would enable polar navigation, enhanced weather forecasts, and the remediation of technogenic hazards.

Geostationary satellites continuously observe the same area as it moves through their field of view. Their contribution to amplification monitoring is, however, limited by large distortions in the field of view in high latitudes. Geostationary satellites are more for monitoring more distant impacts of the amplification in the sub-Arctic or mid-latitude continental areas, where they track snow cover changes.

Data. To date, several important climatic-quality data sets have been developed on the basis of remote-sensing data products. Since the accuracy of the data sets critically depends on high-quality satellite data, ESA CCI utilizes the Global Space-based Inter-Calibration System for bias intercalibration of level-1 data; this system calibrates geolocated measurements of radiances and other characteristics prior to the retrieval of geophysical variables [68]. The ESA CCI ESVs and the European Union's Earth Observation Program Copernicus Climate Change Service (C3S) have benefited from the systematic analysis of climatic-quality satellite data set requirements developed in several subsequent projects, e.g., in the Quality Assurance for Essential Climate Variables prototyping system [69]. An example of this production and validation system that was implemented for the derivation of long-term ice albedo products from MODIS data can be found in [70]. The main requirement for such climatic-quality data sets is that they should be free of multiyear fragmentation, be continuous in time, and be consistent in quality. A triple-collocation method has demonstrated promising results in several ESA CCI projects [71]. Geographically, the data sets should cover the whole Arctic or at least its important regions, e.g., the Barents Sea [72]. Our analysis of sea ice transitions suggests that the temporal coverage should include the critical years between 2000 and 2015.

At present, there is a large diversity in the long-term climatic-quality satellite data products available at different stages of their development [3]. Cross-product validation and calibration are still important issues for the remote-sensing community. The most actively used climatic-quality products in amplification studies are listed in Table 2

Table 2. Actively used climatic-quality remote-sensing products complementing the essential climate variables from ESA CCI.

Product Name (abbreviation)	Accessibility	Reference
Multiple variable products		
MODIS data products	Moderate Resolution Imaging spectroradiometer *https://modis.gsfc.nasa.gov/data/dataprod/*	[30]
Temperature		
UAH MSU/AMSU	University of Alabama-Huntsville (UAH) MSU/AMSU Mean Layer Atmospheric Temperatures, version 6 *https://data.globalchange.gov/dataset/university-alabama-huntsville-uah-msu-amsu-mean-layer-atmospheric-temperatures-version-6*	[73] [65]
SST	Arctic Ocean—Sea and Ice Surface Temperature REPROCESSED *https://data.marine.copernicus.eu/product/SEAICE_ARC_PHY_CLIMATE_L4_MY_011_016/description*	[24]
Cloud and radiation budget characteristics		
CLARA-A2	Cloud, Albedo, and Surface Radiation data set from AVHRR data, second edition https://wui.cmsaf.eu/safira/action/viewDoiDetails?acronym=CLARA_AVHRR_V002	[74]
CERES EBAF	Clouds and the Earth's Radiant Energy System (CERES) Energy Balanced and Filled (EBAF) Top-of-Atmosphere (TOA) edition-4.1 data product *https://asdc.larc.nasa.gov/project/CERES/CERES_EBAF-TOA_Edition4.1*	[75]
PATMOS-x	NOAA's Pathfinder Atmospheres, Extended program (PATMOS-x), v6.0 *https://doi.org/10.7289/V5X9287S*	[76]
APP-x	Extended Advanced Very High-Resolution Radiometer (AVHRR) Polar Pathfinder (APP-x) *https://www.ncei.noaa.gov/data/avhrr-polar-pathfinder-extended/access/*	[77,78]
Sea ice and snow cover characteristics		
NOAA CDR – Rutgers	NOAA Snow Cover Extent Climate Data Record (CDR) Rutgers University Global Snow data set *https://climate.rutgers.edu/snowcover/*	[79]
EUMETSAT OSI SAF v2.0	*https://osi-saf.eumetsat.int/about/access-data*	[80]
Goddard Bootstrap (SB2) and NASA Team (NT1) data sets	National Snow and Ice Data Center (NSIDC): the NASA Team (*http://nsidc.org/data/nsidc-0051*) and Bootstrap SB2 (*http://nsidc.org/data/nsidc-0079*)	[81]
PIOMAS	Polar Science Center sea ice data *http://psc.apl.uw.edu/research/projects/arctic-sea-ice-volume-anomaly/data/*	[82]
Land cover and vegetation productivity		
GIMMS3g	Global Inventory Modeling and Mapping Studies	[66,83]

	https://climatedataguide.ucar.edu/climate-data/ndvi-normalized-difference-vegetation-index-3rd-generation-nasagfsc-gimms	[84]
MEaSUREs	MEaSUREs Global Record of Daily Landscape Freeze/Thaw Status, version 3 (NSIDC-0477) https://nsidc.org/data/nsidc-0477/versions/3	[85]

Methods. This synthesis study utilizes only results that have already been published in literature. We focus on the interannual climatic variability and climate change trends captured in long-term satellite data sets. Our methodological goal is narrowed towards understanding whether satellite observations have captured important transitions in the Arctic climate system—those transitions that have resulted in the emergence of the exceptional amplification in the 21st century [19,34]. Although the amplification was discovered several decades ago [86,87], also through satellite observations [13,88], its emergence in surface records and other environmental indicators remained debated [89–91]. Specifically, the extension of products from the Satellite Application Facility on Climate Monitoring (CM-SAF; www.cmsaf.eu) to the Arctic has increased the quality and diversity of amplification studies [80,92]. CM-SAF is a component of the EUMETSAT activities that provides remote-sensing products derived from meteorological satellites. CM-SAF remote-sensing products provide important data on key variables related to the Arctic amplification, such as surface temperatures, the extent of sea ice, and cloud cover. CM-SAF computes daily and monthly means of various cloud parameters with a horizontal resolution of 15 km. The computations are based on cloud products derived from the AVHRR instrument onboard polar-orbiting satellites and from the SEVIRI (Spinning Enhanced Visible and InfraRed Imager) instrument on the geostationary satellites.

3. The Synthesis

The current physical understanding of the amplification. Energy-balance models of the earth's climate system clearly relate the emergence of the apparent amplification to the changing heat capacity of the system, i.e., to the capacity to retain heat in the lower atmosphere and in the upper ocean/soil levels [93]. These models have revealed that the amplification emerges as the atmospheric fast mode in the meridional response to anthropogenic climate change. Enhanced heat transport towards the Arctic is a precursor driving sea ice melt and the eventual transition to a seasonally open-water Arctic Ocean. This indicates that the amplification can be seen as a response to the redistribution of heat sources and sinks on the planet [94]. In this way, accepting Manabe and Strickler's arguments [95], the amplification should not distort much of the top-of-the-atmosphere (TOA) radiation balance. On the contrary, a prominent effect on the surface energy balance is expected, as the surface is largely decoupled from the higher atmospheric layers in the stable Arctic atmosphere. Satellite observations clearly identify such a fingerprint of the dynamic Amplification drivers. Finally, both climate modeling and results of reanalysis studies found that the apparent amplification has accelerated when the local surface feedback was unlocked after the transition to seasonal sea ice cover [14,15,96]. This is when the surface recouples to the lower atmosphere. The fact that the amplification emerges in response to so many different drivers suggests that it is a robust global climate response independent of applied forcing and feedback details [9,14].

At present, the research community has created a physically consistent conceptual picture of the amplification [9]. The amplification is initiated by the atmospheric dynamics, but it is shaped and enhanced by interacting local physical processes and feedback. Climate simulations suggest the following chain of causality. Meridional atmospheric transport increases moist-static energy in the Arctic troposphere, which drives sea ice variability [97]. Initially, the atmospheric warming has little observable effect on the extent of sea ice and on surface temperatures, as multiyear ice has survived melting seasons [98].

By the year 2000, however, multiyear ice largely disappeared from the central Arctic and Eurasian shelf [42,44]. This outrunning thinning and reduction in multiyear ice was explained through a growth-thickness negative feedback mechanism [99]. Variability in the seasonal sea ice cover has increased [100]. This has unlocked mechanisms of summer heat accumulation in newly open surface waters with subsequent effects on autumn and winter temperatures [101]. The apparent amplification has been unlocked. Several specific physical feedback mechanisms trap further warming near the surface, enhancing its environmental impact. The most pronounced changes are then observed in the areas of the most recent sea ice and snow cover retreat, such as the marginal sea ice zone [19] and the forest–tundra interface [7]. A schematic illustration in Figure 3 provides a general overview of the dynamics and physics of the amplification under surveillance of the ESA satellite fleet.

Emergence and location of the apparent amplification. The current understanding maintains that the amplification developed for a long time in the free (lower) atmosphere, before it finally emerged onto surface climate records. Figure 4 displays this development in the UAH MSU TLT (lower atmosphere) data set. Time series of the Arctic and Hemispheric temperature anomalies, Δ_{AA}, began diverging in the 21^{st} century, with the largest difference noted around 2005 and then again after 2015. The reanalysis data reveal that the contemporary amplification took off in 1990s [22]. Satellites (AVHRR data set) reveal the surface warming trends at latitudes above 64°N of ~0.69 ± 0.06°C dec^{-1} compared to ~0.17°C/dec^{-1} globally from 1990–2010 [13]. The largest trends are found in the areas of active seasonal sea ice loss. The sea ice surface temperature and the sea surface temperature in the Arctic show smaller trends of 0.47 ± 0.06°C dec^{-1} and 0.09 ± 0.01°C dec^{-1}, correspondingly.

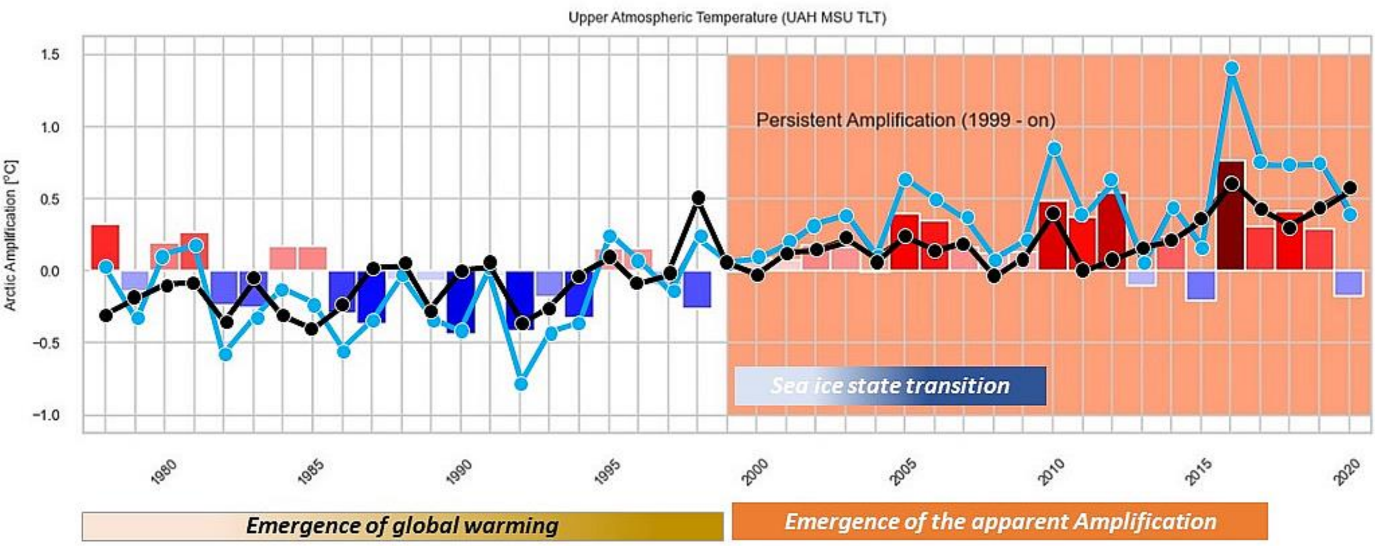

Figure 4. The amplification in the satellite observations (the lower troposphere UAH MSU TLT data set) with sketched periods of the apparent amplification emergence. The blue line shows the Arctic temperature anomalies; the black line shows the Northern Hemisphere temperature anomalies; the colored bars show the amplification (the difference Δ_{AA} between the lines).

Surface state transition caused by sea ice retreat. Monitoring of sea ice provides a spectacular example of satellites' contribution to the radical rethinking of Arctic climate change [17,42]. A wide variety of satellite instruments provide data for sea ice monitoring [5,102]. Beginning with monitoring of the extent of sea ice [81,103], remote-sensing data products have gradually begun to provide for sea ice thickness since 2005 [44], as well as other derivative characteristics of the sea ice cover [42,102], including compactness and lead fraction [104,105]. Satellites with low spatial and high temporal resolution provide synoptic information about the Arctic sea ice cover, age, motion, and timing of retreat and advance.

Towards the end of the 20th century, global warming has been progressing without visible differences in its pace at low and high latitudes. The warming pace began to diverge only when sea ice had retreated over large areas in the Barents Sea and the Eastern Arctic. Satellites were able to capture a critical transition in both the extent and thickness of sea ice [106]. Between 2005 and 2007, the mean residual (October–November) sea ice thickness rapidly dropped by 1 m (about 50%), manifesting a transition from multiyear to seasonal ice cover [13], and the age-based sea ice volume decreased by around -411 km^3 yr^{-1} [43]. Changes in sea ice thickness contribute more this volume change than changes in sea ice area. The 15-year satellite record depicts an ice volume loss of 4305 km^3 and 7695 km^3 in winter (February–March) and autumn (October–November), respectively. These numbers suggest that 30% to 40% of the total sea ice volume and >70% of the multiyear ice volume have been lost already. The major transition from about 4×10^6 km^2 to less than 2×10^6 km^2 of multiyear sea ice occurred between 2005 and 2010. Figure 5 shows the changes in the sea ice extent (SIE) derived from the OSI SAF Sea Ice Index product. This transition is detected by combining data products from NASA Ice, Cloud, and land Elevation Satellite (NASA ICESat) over 2003-2008 and the European Space Agency Earth Explorer Cryosphere Satellite 2 (ESA CryoSAT-2) from 2010 onward. The gap from 2008–2010 was unfortunate, however, as it occurred in the middle of the main multiyear sea ice decline period [44]. Data from the QuikSCAT (1999–2009) and MetOP ASCAT (2009–2018) scatterometers indicate more than a 50% decline in multiyear sea ice coverage [44], with a rapid decline in the multiyear ice area and volume that happened over just a few years (see Figure 5). The most used climatic quality sea ice data sets agree on ice patterns and the overall extent and trends [81]. A disagreement remains when sea ice characteristics, especially ice concentration distributions, in the marginal ice zone and adjacent regions are considered.

The role of sea ice transition is further emphasized in an analysis of the seasonality of the trends. The amplification reveals a strong seasonal cycle, see Figure 6. The most significant changes develop when the surface freezes or melts, notably during September, October, and November (SON) due to the persistent shift in the melting/freezing onset. The mean SON trends in 12 reanalysis data sets are greater than +5 K from 1979–2017 [107]. The mean melting season (June, July, August) trends are less than +1 K from 1979–2017.

As sea ice retreats, the sea surface temperature (SST) in the Arctic begins increasing as well [6,108]. The mean August SST is the most appropriate representation of Arctic Ocean warming. The highest mean August SST (6–9°C) is observed in the southern Chukchi and Barents Seas.

The warming of the Arctic SST is, however, in its initial stage. Yet the ocean impact is growing. Satellite-based analysis of sea ice loss suggests the rising influence of ocean fluxes [109]. One modeling study [110] attributed about 1°C near-surface warming in winter to the thinning of sea ice, which corresponds to about 37% of the amplification in the marginal sea ice zone. Another study [111] argued that increasing ocean heat inflow leads to thermodynamic recoupling between the ocean and the atmosphere, and this might account for about 80% of the amplification by 2100.

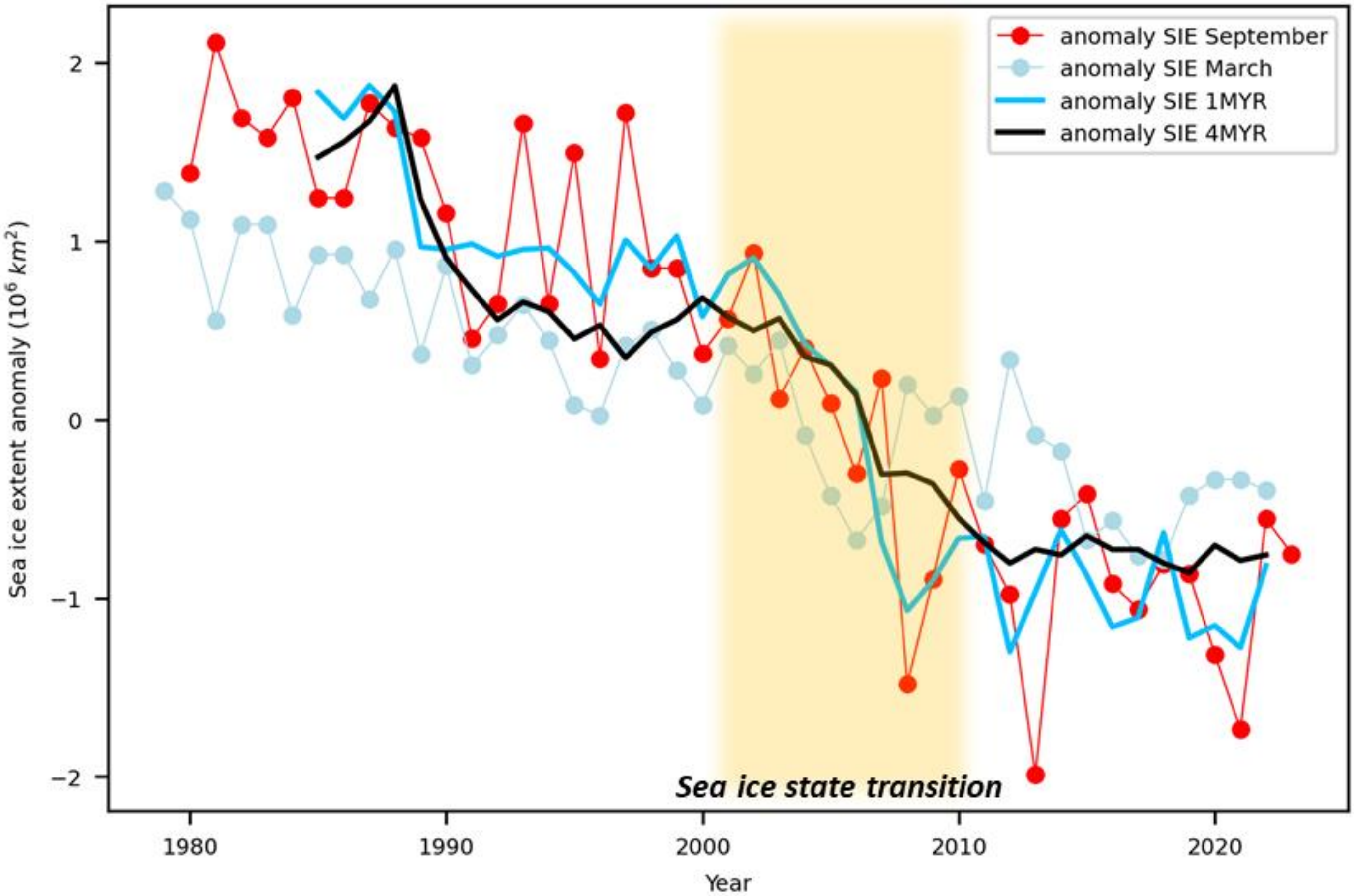

Figure 5. Changes in the Arctic sea ice extent (SIE). The total September and March SIE anomalies are taken from the OSI SAF Sea Ice Index v2.1 (available at https://osisaf-hl.met.no/v2p1-sea-ice-index, last accessed 05.01.2023) [80]; the reference period is 1989–2021. All data are based on passive microwave sensors (the SMMR, SSM/I, and SSMIS); the multiyear (older than one year, 1MYR) and old (older than 4 years, 4MYR) SIE anomalies are taken from NSIDC [112], see more details in [43]. SIE is defined as the area covered with more than 15% of sea ice.

Surface-state transitions caused by snow cover retreat. The longest satellite observations (since 1966) exist for snow cover [10,25]. The NOAA Climate Data Record (CDR), also known as the Rutgers snow cover data set, has been digitized from snow cover maps at a spatial resolution of 190.6 km at 60N [79]. Since 2004, both the spatial resolution and quality of this record have been greatly enhanced by MODIS and VIIRS data streams (0.5 to 1 km resolution, respectively). The European Space Agency (ESA)'s GlobSnow product has an intermediate (25 km) resolution, which is generally adequate for homogeneous surfaces in the Arctic. The snow cover is in retreat in the Arctic, but trends remain controversial and dependent on the selected period and season. Estilow et al. [79] showed that the extent of hemispheric seasonal average snow cover increases in fall and winter but decreases in spring and summer. The snow cover duration is decreasing by 5–6 days per decade over the Northern Hemisphere. The snow water equivalent (SWE) determines the amount of heat needed to melt snow, and thus, it is important for the emergence of the amplification. Results for the SWE trends from the 36-year passive microwave record (1980–2015) suggest that the hemispheric SWE is decreasing. However, at regional scales, the trends are less certain and are highly variable between products. New satellite missions with the ability to retrieve snow water equivalents are needed to fill the gap in quantitative information. The Copernicus Global Land Cover service provides SWE for the northern hemisphere at a 5 km resolution (https://land.copernicus.eu/global/products/swe).

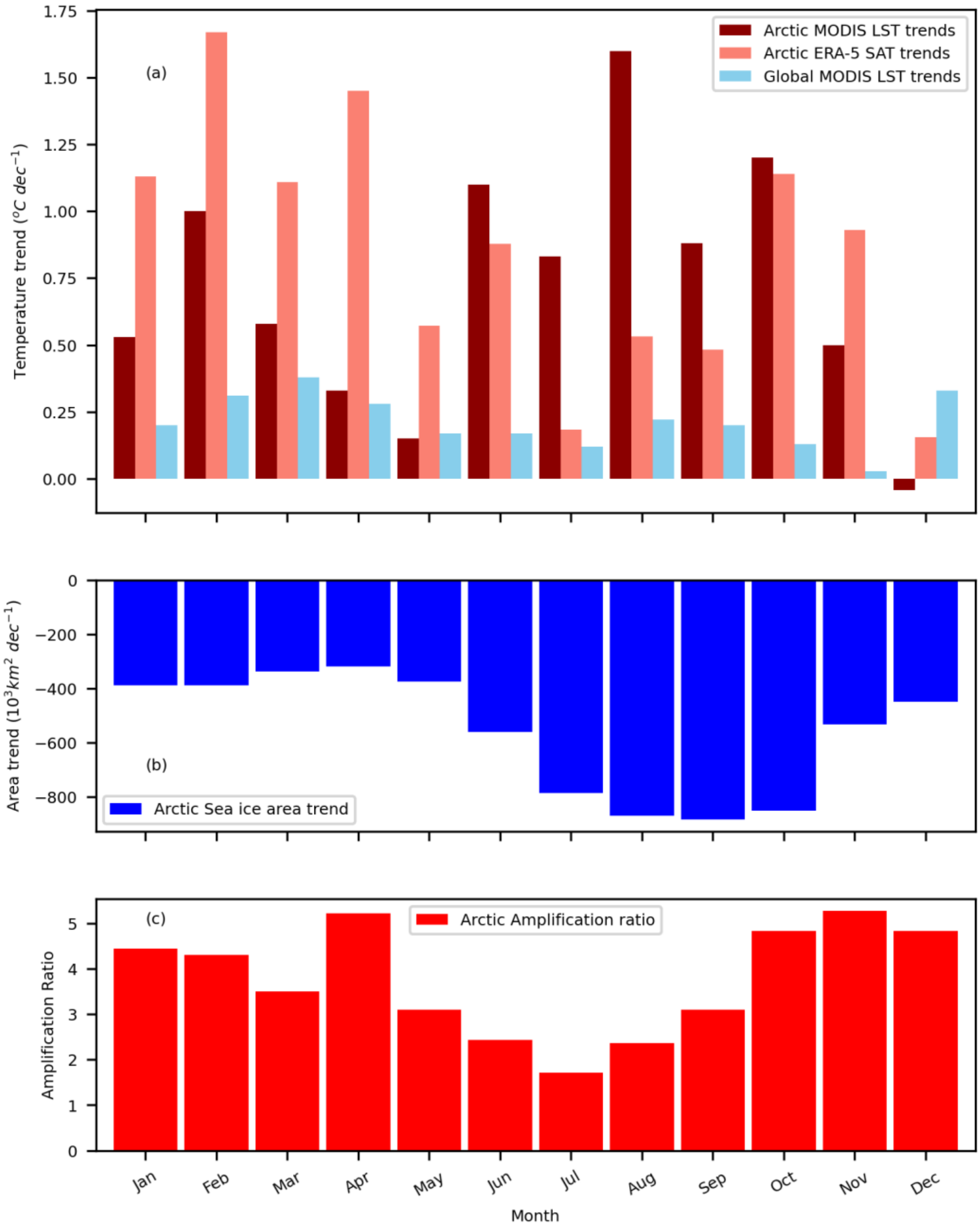

Figure 6. Monthly variations in Arctic climate trends. (a) Land temperature (LST) trends from MODIS LST data set and the surface air temperature trend from ERA-5 reanalysis from 2001–2020 [40]. (b) Sea ice area trends from 1979–2019 [113]. (c) Arctic amplification ratio from 1979–2021 averaged over three observational data sets (Berkeley Earth, Gistemp, HadCRUT5) and the ERA5 reanalysis [34].

Surface–atmospheric coupling effects. The Arctic is one of a few regions (other regions are collocated with ocean upwelling zones) where weak surface–atmospheric coupling controls the climate sensitivity [95].

Satellite observations can be used to estimate the characteristics of the vertical turbulent mixing, surface layer coupling, and effective heat capacity of the climate system [114]. However, such data products are still in their infancy. A promising algorithm looks at aerosol backscatter [115]. It utilizes a threshold at which the backscatter signal exceeds the clear atmosphere signal by a small arbitrary value or vertical gradients in a lidar backscatter profile. More sophisticated detection methods have been suggested as well [116]. The CALIOP (Cloud-Aerosol Lidar with Orthogonal Polarization) instrument onboard the CALIPSO mission was also used [117,118]. Another potentially useful data set is provided by GPS Radio Occultations (GPS-RO) [119], which are more numerous and less sensitive to clouds. The GPS-RO algorithms typically define the boundary layer height as a level of the most negative moisture gradient [120]. During the winter months (December–February), when the total precipitable water in the troposphere is at a minimum, a fairly straightforward algorithm based on temperature inversions can be used [121]. The shallow Arctic boundary layer is a challenge for the GPS-RO retrieval. Ding et al. [122] showed that the 10-year retrieval has a low vertical resolution and accuracy, which could be critical for the detection of the boundary layer height in high latitudes. Temperature profile methods could be also used for the retrieval of the boundary layer height. In the Arctic, however, temperature inversions are of radiative origin and could be unrelated to vertical mixing. In addition, there is still no synthetic data product for lower atmosphere temperature inversions. The existing data sets, e.g., a 17-year time series (1980–1996) of clear-sky temperature inversions derived from High-Resolution Infrared Radiation Sounder (HIRS) data [38], do not cover the emergence period.

Turbulent fluxes are also important for the assessment of the surface energy budget, air–surface coupling and moisture, greenhouse gases, and aerosol exchange. The remote sensing of turbulent fluxes is a rapidly developing application of the earth's observations. Significant progress has been achieved in development of turbulent flux products over the global open ocean [71]. A corresponding development in the Arctic domain, however, has met with considerable difficulties. Turbulent fluxes here are influenced by sea ice, frequent overcast cloudiness, high wind speeds, low winter temperatures, and a small temperature contrast between the surface and cloud layers. Surface heterogeneity and the presence of sea ice leads, in particular, might greatly enhance the fluxes [123]. Qu et al. [124] derived turbulent fluxes from leads at different scales using a combination of surface temperatures and lead distribution from remote-sensing images (Landsat-8 TIRS and MODIS) and meteorological parameters from a reanalysis data set. A fetch-limited model applied to thermal images and wind data estimates the fluxes to be more than 40% larger than those of the homogeneous sea ice surface.

Arctic cloudiness effects. Arctic cloudiness is undoubtedly the major wildcard in amplification assessment and understanding [47]. The cloudiness effect is twofold. Clouds distract optical satellite surface observations and data retrievals, and clouds play an active and still poorly understood role in forcing the amplification on all scales. Strong connections have been found between cloud cover changes and dynamical patterns of the heat inflow into the Arctic [125]. Figure 7 compares interannual variations in the total cloud cover in the Arctic and its effect (forcing) on the longwave radiation balance at the surface, as obtained from two satellite data products. The recent decade has witnessed both enhanced cloud cover and its surface heat forcing.

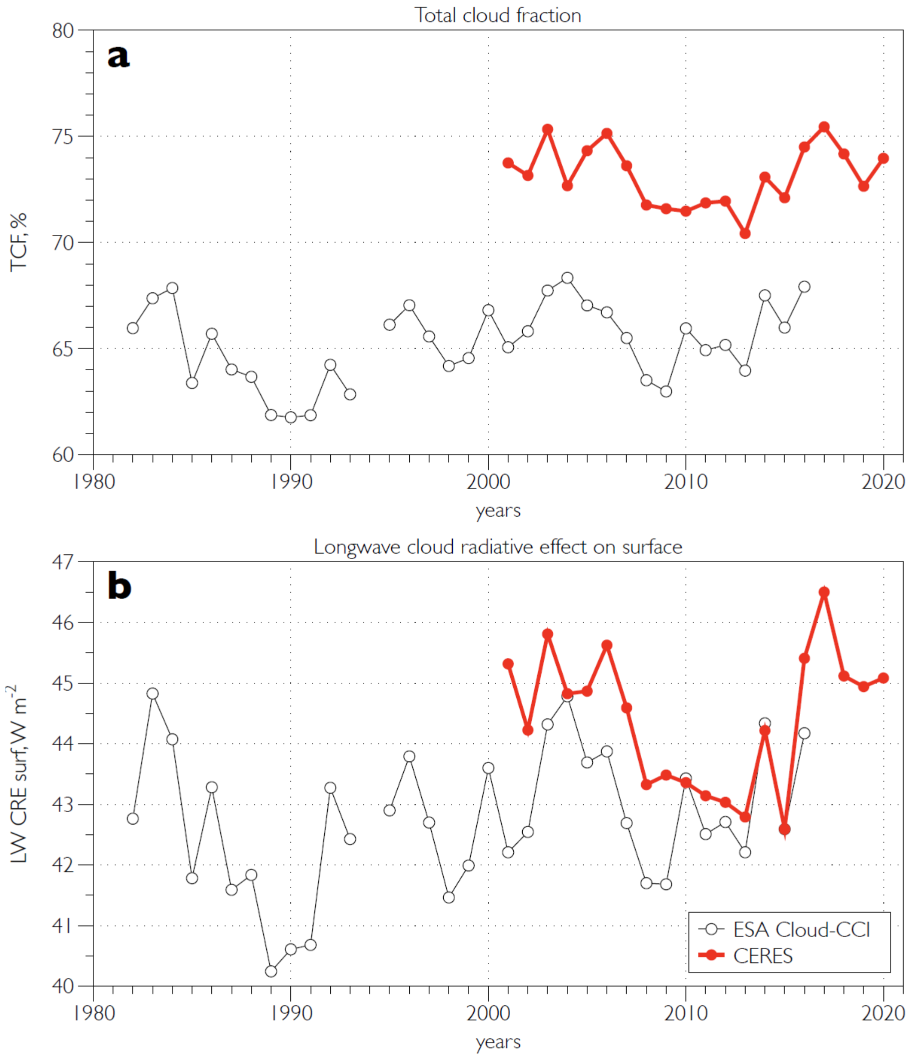

Figure 7. Variations in the total cloud cover (a) and the longwave cloud radiative effect on the surface (b) obtained from ESA Cloud-CCI and CERES data products.

Satellite observations are essential in studies of Arctic cloudiness and its impact [32,126,127]. Today, almost 40 years (1982 on) of satellite cloud observations are available [47]. Currently, four long-term climate data records (data sets) exist that are exclusively based on AVHRR data. One is a CM SAF Cloud, Albedo, and Surface Radiation data set from AVHRR data, second edition (CLARA-A2). It applies a hierarchical decision tree thresholding method to retrieve cloud properties [74]. The other data set—the NOAA's Pathfinder Atmospheres, Extended program (PATMOS-x)—is based on a naïve Bayesian method [76]. The third is the Extended Advanced Very High-Resolution Radiometer (AVHRR) Polar Pathfinder (APP-x) [77]. The fourth is the ESA Cloud CCI (version 3) 1982–2017, which uses neural network and optimal estimation techniques to provide cloud property retrievals [128,129].

Satellite cloud data products do not fully agree with each other. A study of 16 cloud climatologies showed that the annual mean total cloud fraction in the region north of 60°N is 0.70 ± 0.03 (over the ocean 0.74 ± 0.04; over land 0.67 ± 0.03) [130]. The average disagreement between MODIS and CALIOP over the whole Arctic reaches 13.1% during daytime and 26.7% during nighttime [131]. This MODIS–CALIOP disagreement has high seasonal dependence; it is the lowest in summer (showing a 10.7% difference in cloud fractions) and the largest in winter (28.0%). MODIS typically under-detects low-level (top height <2 km) and high-level clouds (top height >6 km). Very low and thin clouds (<0.3 km) over sea ice that are detected by MODIS are sometimes not observed or misclassified by

CALIOP. Aside from this, MODIS cloud products perform better over open water than over ice [132]. The main reason for the discrepancies among observations is the difference in cloud detection algorithms, especially when clouds are detected over the ice/snow surface (during the whole year) or over regions with a presence of strong low-tropospheric temperature inversions (mostly in winter).

Arctic cloudiness is particularly challenging for climate models, causing major uncertainties and discrepancies in regional climate change projections. Most models project increasing low-level cloudiness in the region. Satellite observations confirm this tendency [114]. The Arctic was found to be more cloudy in spring (the decadal trend from 1984–2004 is 2.3% dec^{-1}) and summer (0.5% dec^{-1}) but less cloudy in winter (−3.4% dec^{-1}) [33]. More recent studies [133], however, found extensive positive low-level cloud fraction trends over the Arctic sea ice. The strongest trends are found for October and November. Amplitudes of these trends exceed +10% dec^{-1}.

The estimations of the TOA forcing sensitivity give -0.46 ± 0.90 W m^{-2} per each percentage of cloud cover change for shortwave radiation and $+0.14 \pm 0.087$ W m^{-2} per percentage for longwave radiation. The temperature responses to radiative changes vary from 0.25 W m^{-2} K^{-1} in the CLARA A1 data to 0.43 W m^{-2} K^{-1} in the CERES broadband planetary albedo data [53]. Hwang et al. [134] gave estimations of the radiative feedback using CERES/Terra data (2000-2014) of 1.88 ± 0.73 W m^{-2} K^{-1} and 2.38 ± 0.59 W m^{-2} K^{-1} for short- and long-wave radiation, respectively. They found that clouds reduce the albedo feedback by about 50%, from 1.13 ± 0.44 W m^{-2} K^{-1} in clear-sky periods to 0.49 ± 0.30 W m^{-2} K^{-1} in overcast periods. The TOA cloud feedback over 60°–90°N using CERES data remains rather uncertain, ranging from –0.3 to 0.5 W m^{-2} K^{-1} [135]. Kay and L'Ecuyer [136,137] concluded that the clouds over the Arctic Ocean warm the surface by 10 W m^{-2} in annual average and cool the top of the atmosphere (TOA) by −12 W m^{-2}. Philipp et al. [114] analyzed clouds, radiation flux, and sea ice records covering 34 years of satellite observations. These data confirmed statistically significant anticorrelations between sea ice concentrations and the cloud fraction in autumn over melting zones. The net warming effect of clouds was found in late autumn through spring due to weak solar insolation. Thus, an increasing fraction of low-level clouds induces a surface warming trend up to +8.3 W m^{-2} dec^{-1}, causing a prolonged melting season and hindering perennial ice formation. Based on an assumption that the observed decrease in albedo is responsible for the full warming, Pistone et al. [50] obtained a feedback estimation of 0.31 ± 0.04 W m^{-2} K^{-1}.

Excessive cloud cover interferes differently with short- and long-wave radiation. In summertime, when short-wave radiation is available, a reduced cloud fraction allows for additional absorption of the solar energy at the surface and in the upper ocean. In total, Arctic clouds cool the atmosphere by 22 W m^{-2} [137]. The annual average cloud forcing has been changing at a rate of −2.11 W m^{-2} dec^{-1}, indicating a damping effect on the surface warming by clouds [33]. Cloud effects could, however, be offset by a changing surface albedo and radiation balance, as well as by a redistribution of the additional heat between atmospheric layers [51]. The net heating (the warming contribution to the amplification) effect of clouds is still uncertain and remains rather disputable [138]. However, recent additions to the satellite fleet (A-train with CloudSat and CALIPSO) have considerably advanced our knowledge of the Arctic clouds and their climatic impact [137].

Many important issues have been clarified in recent studies [47]. It was confirmed that reduced cloudiness supports the amplification well into the autumn season, when accumulated heat is released [139]. In the wintertime, enhanced low-level cloud fraction traps outgoing long-wave radiation. This trapping is known as cloud optical depth feedback [140]. Observations from the ISCCP, MODIS, and PATMOS-x platforms confirmed that this feedback increases surface warming [141]. The CERES EBAF data set suggests that cloudiness over the areas of sea ice retreat is enhanced, inducing positive radiation forcing [137,142]. Since clouds reduce surface heat loss in the winter season, they are capable of enhancing the amplification.

The Arctic energy budget. Satellite platforms are the most suitable for observing spectral radiance and the energy budget [31]. Therefore, the amplification has gained the largest boost in understanding from climatic-quality data sets of the radiative components of the TOA and surface energy budgets and forcing. The total Arctic energy budget is dominated by a heat deficit of 115.8 W m^{-2} at the top of the atmosphere (TOA) on the annual average [94]. This deficit is larger (-176.9 W m^{-2}) in January but reverts to a small energy gain (12.4 W m^{-2}) in July.

The TOA radiative forcing has been reconstructed using different sensors since the end of 1970s [31]. The CERES data set (2000-2018) indicates only a statistically insignificant Arctic TOA response of -0.19 ± 0.44 W m^{-2} K^{-1} (in high sea ice concentration (SIC) periods) to -0.15 ± 0.16 W m^{-2} K^{-1} (in low SIC periods) [48]. Thus, the TOA radiative response in the amplification domain has remained nearly stable during the recent period, which is in agreement with model-drawn conclusions [14].

Changes in the regional surface albedo have a strong impact on the heat absorption and redistribution in the Arctic. The long-term darkening of the Arctic surface due to sea ice loss has been observationally confirmed; the mean surface albedo has been reduced from 0.52 to 0.48 since 1979 [50]. Over 28 years of homogenized satellite data (CLARA-A1-SAL product; 1982-2009), the mean albedo of the sea ice cover has been decreasing at 0.029 ± 0.011 dec^{-1} [49]. As sea ice and snow cover retreat, the total Arctic surface albedo has decreased over 1982–2014 at rates of 1.25 ± 0.34 (CLARA A1) and 1.51 ± 0.41 % dec^{-1} (APP-x) [143]. This has caused moderate changes in the radiative fluxes and forcing. Using the CLARA A1 data product, Cao et al. [53] found that sea ice loss has resulted in a 0.20 ± 0.05 W m^{-2} decrease in radiative forcing, yielding a sea ice albedo feedback strength of 0.25 W m^{-2} K^{-1} for the Northern Hemisphere and 0.19 W m^{-2} K^{-1} for the entire globe.

4. A Broader Impact of the Amplification

Impacts on extremes. Interest in the amplification is maintained by its impact on the marine environment, the biosphere, and the cryosphere. The amplification changes not only the mean values of ECVs but also induces a broad spectrum of weather extremes and environmental hazards [144]. Extremes are becoming new normals in the changing Arctic [8]. Amplified warming literally means more intensive and more frequent heat waves in the Arctic, such as those observed in 2012, 2016, 2019, and 2020 [145]. The effects of sea ice retreat, snow cover reduction, and soil carbon release could be felt worldwide [146], though they are perhaps not as straightforward as it has been previously suggested [147]. At the same time, there is no consensus on the impact of the amplification on mid-latitude weather extremes [148]. Synoptic activity in the mid-latitudes likely enhances the amplification; poleward winds are stronger in years of reduced sea ice concentration, increasing the atmospheric (surface oceanic) poleward heat flux by up to 25% and accelerating sea ice retreat [149]. However, the amplification likely has an insignificant impact on synoptic activity [150].

Impacts on ecosystems. The amplification impacts Arctic ecosystems (both their composition and productivity) strongly. The most informative data products systematically quantify changes from earlier baselines [90]. The longest running data product combines more than 40 years of satellite observations since 1981 in the Global Inventory Modeling and Mapping Studies (GIMMS) [66,83]. Vegetation indices in GIMMS isolate signals of vegetation productivity by emphasizing reflectance in different parts of the radiometric spectrum. However, the indices are not developed in the polar context [7]. The relevant issues here, for instance, are a low sun angle, an abundance of surface water, and a low or high surface contrast. Other climatic-quality products include: VIP3 (Vegetation Index and Phenology, version 3), LTDR4 (Long-Term Data Record, version 4), SPOT-VGT (Système Pour l'Observation de la Terre VEGETATION), and the MODIS data set [30]. These data products still have trend discontinuities, as sensor shifts potentially introduce uncertainties and artifacts in data records [151]. Spatial fragmentation of the pixel-based trends creates difficulties for regional trend aggregation [152], so that a trend detection methodology needs more attention [153]. Satellite products also suffer from inadequate sensitivity to detect changes; known problems are related to aliasing from decreasing snow cover and increasing leaf area, atmospheric contamination, orbital drift, and sensor replacements [83]. At present, the EU Sentinel missions [154] have significantly improved monitoring of the terrestrial ecosystem, introducing a 10–60 m spatial resolution and a potential revisit time of five days. The development of hyperspectral missions such as the EnMAP, FLEX, and HyspIRI is expected to deliver richer functionality and accuracy of information. In recent years, attempts to retrieve more diverse traits, such as plant heights, have been presented [155]. The retrieval combines C-band SAR and multispectral vegetation indices, especially through the acquisition strategy of Sentinel-1 and 2.

Remote sensing has already revealed longer growing seasons (up to 20 days longer over the past decade) and increased annual biological production (greening) of the northernmost bioclimatic zones of tundra and forest–tundra [156]. In total, seasonal biological productivity has increased for 42% of northern vegetation, which translates to a 21% gain in productivity between 1982 and 2014 [57]. Only 2.5% of northern vegetation shows browning, which corresponds to a 1.2% loss of productivity.

Impacts on marine biology. Sea ice retreat has improved illuminance, followed by increasing temperatures in upper, biologically productive layers. More stormy weather, higher waves, and enhanced inflow of Atlantic water enrich the productive layers with nutrients. Satellites are witnessing growing primary production, which extends further north and east in the marginal Arctic seas [26,157]. Areas of marine species, from algae and fish to birds and polar bears, have been moving northwards, with implications for the entire food web and leading to an increasing number of fishing vessels visiting Svalbard. Satellite platforms are the main tool to monitor marine ecosystems, providing for the onset and peaks of the annual spring and summer algae blooms as well as for their extent and phenology, both in open waters and under sea ice. Fishery fleet activity can be also monitored. The combined use of SAR and AIS data will provide information on changes in the catch pattern of the fishing fleet in Arctic waters. The ESA contribution has been politically recognized as an essential basis to sustain fisheries in the Arctic Ocean [158].

Impact on soils and permafrost. Following the amplification and land cover changes, warming begins to penetrate in active soil layers and permafrost [159]. The changes in permafrost could be monitored from space using direct and indirect methods. Indirect methods utilize diverse signatures left on terrestrial morphology, hydrology, and biology [29,160]. Such surface changes could be related to the occurrence of certain vegetation types [161] or to the disappearance or shrinkage of lakes [162]. The proxy data may be utilized to extend global permafrost products back to the 1980s or to even earlier periods.

A more direct approach utilizes the land surface temperature and its derivatives in connection with soil temperature modeling. The model complexity and remote-sensing contributions may vary. A number of auxiliary input parameters might be involved. A simple frost-and-thaw index approach was commonly used in earlier works, but later, a more computationally extensive approach began to dominate [163]. Permafrost monitoring with the MODIS LST input was applied by Marchand et al. [164]. This approach is followed in the GlobPermafrost project [56]. It estimates permafrost distribution using an equilibrium state model for the temperature at the top of the permafrost (TTOP model) for the 2000–2016 period. The Copernicus Sentinel-1 and -2 missions provide information on changing topography (land surface slumps, erosion related to thawing permafrost, surface depressions, shrubification), whereas missions carrying thermal sensors (Sentinel-3) assess changes in the land surface temperature. Information on snow conditions and land cover can be used as a proxy for soil properties. Both snow and soil regulate heat transfer and thus determine the impact of the amplification on the frozen soil beneath. Park et al. [54] inferred the extent of permafrost from satellite microwave data of the daily landscape freeze–thaw status over 30 years (1980–2009). The data set is presented in Kim et al. [85]. The extent of permafrost has been declining since 1980 at a rate of 0.33 million km^2 dec^{-1} ($p < 0.05$), but this decline has seemed to accelerate since 2004.

Impact on the Arctic ice sheets and glaciers. Due to the vast time scale difference, it is not a simple question as to whether the amplification has already imposed its impact on the Arctic ice sheets and glaciers. Satellite data reveal a robust decline in the Greenland ice mass since the 2000s. The IMBE team [58] published a data set that compares and combines 26 individual satellite measurements of changes in the Greenland ice sheet mass balance. The ice sheet remained nearly in balance in the 1990s, but annual ice losses have risen since then. The peak loss was recorded in 2011, when it reached 345 ± 66 billion tons. The total loss between 1992 and 2018 was 3,902 ± 342 billion tons of ice, driving the mean sea level up by 10.8 ± 0.9 mm. Despite its significant ice sheet loss, Greenland and the surrounding seas do not exhibit a strong amplification, perhaps due to an increasing influx of ice in the adjacent waters. A review by Cooper and Smith [60] synthesized remote-sensing methods and key findings for the Greenland ice sheet ablation zone. Observations for other, smaller glaciers have provided more diverse results [165].

Impacts on society and humans. Although still wild and remote, the Arctic is increasingly touched by human activity. The Sentinel-1 and -2 satellites have improved the mapping of Arctic settlements and infrastructure [61,62]. Local human disturbances around settlements, mining fields, and transport routes are gradually merging into a pan-Arctic network of modified land cover types. The slow recovery of soils and vegetation increases the footprints of any disturbances, even minimal artificial ones. High-resolution satellite imagery has helped in tracking human footprints over decades, e.g., in northern West Siberia, where the exploration of vast hydrocarbon deposits has been extensive since 1970s. Holistic, interdisciplinary studies of human-induced disturbances include the analysis of diverse satellite imagery and remote-sensing data products [166]. The extensive transformation of disturbed land patches has been documented.

Sizov et al. [167] gives an illustrative example of northern forest advance in northern West Siberia. They compared high-resolution satellite images taken over the last 50 years (1968–2018). The study clearly demonstrates the widespread advance of alternative ecosystems (forest) on damaged land patches that replace tundra ecosystems in their traditional ecotone (Figure 8). Generalizing this example, enhanced greening has been revealed in the MODIS NDVI data around the majority of Arctic towns [168].

Figure 8. Afforestation of a burned tundra area in northern West Siberia. The left image was taken by Corona/KH-4b, 21.08.1968, the right image by Resurs-P, 28.09.2016. Source: [168].

Following global economic and political trends regarding Arctic development, the Arctic population is experiencing significant changes [169]. The amplification creates both risks and opportunities. On the one hand, sea ice retreat, increasing land productivity, and less severe winters improve access to remote areas and resources in the Artic. On the other hand, an active soil layer and permafrost warming lead to weakened ground stability under infrastructure [2], destroyed roads, and other detrimental effects [170]. Satellites have monitored human-induced changes and effects since the 1960s. There are several important issues for satellites to follow up on, namely, coastal erosion [61], the stability of settlements on the permafrost [171,172], and monitoring of the environmental pollution [173].

5. Conclusions and Perspectives

Responding to the global issue of anthropogenic climate change, the European Space Agency (ESA) has undertaken the Climate Change Initiative (CCI) to exploit the full potential of long-term global satellite observations. The ESA CCI essential climate variables (ECVs) cover more than 40 years of monitoring the earth from space and provide climatic-quality data sets for the investigation of climate phenomena in development [3]. Data sent by the ESA, NASA, and some other satellite platforms are utilized to create a variety of ECV records. Both the advantages and challenges of the ESA CCI projects are related to the need to fuse data information from different sensors working on different satellite platforms with different spatial, temporal, and spectral resolution. Nevertheless, since the emergence of profound climate change in the Arctic has been delayed by the transition of the sea ice state, ESA CCI climatic-quality records have captured the amplified and accelerated climate warming in the Arctic and its widespread influential effects and impacts. These linkages are summarized in Figure 9.

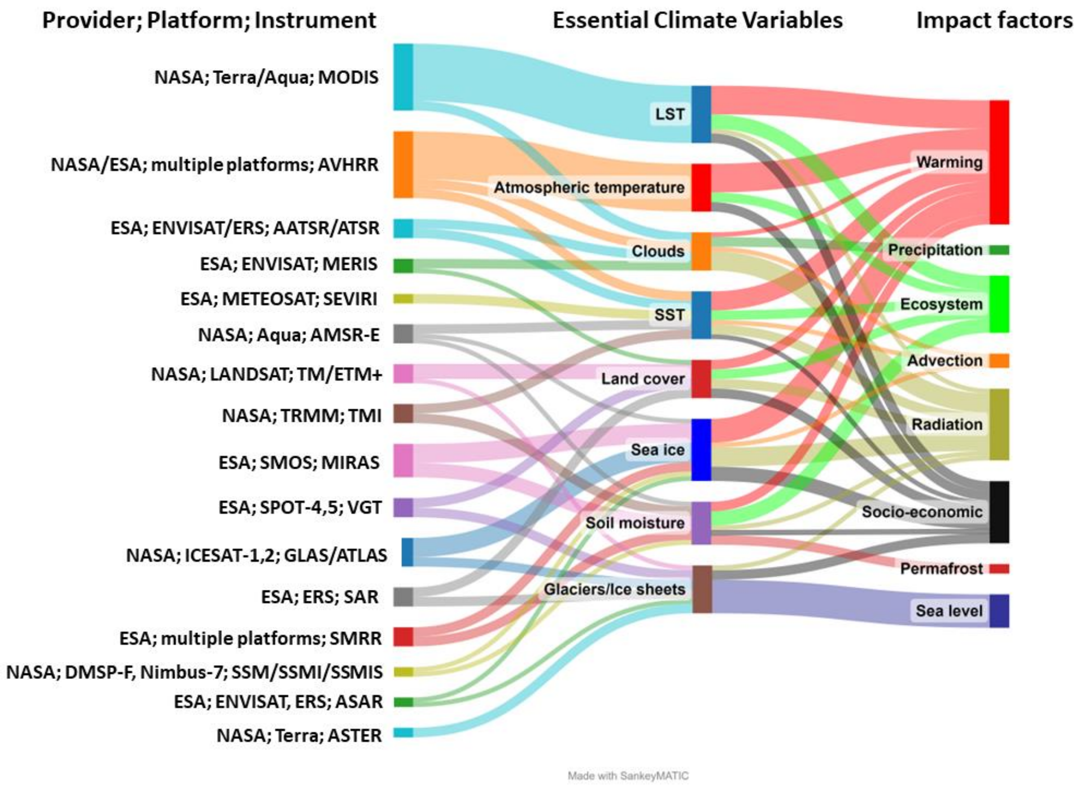

Figure 9. Primary satellite sensors contributing to the amplification ECVs in the ESA CCI program. The diagram combines presentations in several publications [5,12,68,80]. A complete description for each ECV is available at https://climate.esa.int/en/.

Satellite observations are indispensable for crystallizing a new physical paradigm for the amplification. Although this paradigm benefits from model sensitivity and process studies, such modeling efforts would not be feasible without satellite information in native resolution on the characteristics of sea ice, snow cover, clouds, vegetation, albedo, and TOA radiative fluxes—all of these characteristics are poorly reproduced in unconstrained model runs. Specifically, satellite observations have been essential in revealing the link between sea ice cover and the apparent (surface layer) amplification. They revealed the spatial relocation of the amplification core from the northern continents to the marginal sea ice zone (e.g., the Barents-Kara Sea region) as soon as multiyear sea ice cover had disappeared.

This synthesis draws a broadly consistent picture of the amplification and its impacts derived from the ESA CCI ECVs and other collections of climatic-quality remote-sensing data products. At the same time, we have to agree with a critical judgement of satellite observations: "*While suitable for detecting overall change, the current capability [of satellite observations] is inadequate for systematic monitoring and for improving process-based and large-scale understanding of the integrated components the cryosphere, biosphere, hydrosphere, and atmosphere*" [5]. There is future potential in multi-sensor/data and synergetic applications of satellite and in situ data to be used in combination with numerical modeling. Those still-existing gaps in ECVs for amplification monitoring will be reduced by new ESA satellite missions [67].

Perspectives on the future amplification. The amplification is a robust response to climate forcing. Historical observations and climate reconstructions have revealed periods of amplified and accelerated temperature trends in the Arctic's past [174]. Model simulations suggest that the amplification will proceed into the future. At the same time, the amplification will not develop as a steady process. Will it vanish as the Earth's climate system approaches its new, warmer equilibrium? Climate models suggest that it will decrease already by the end of the 21st century [175], owing largely to the disappearance of summer sea ice in the Arctic and the equilibration of the global radiation response in the climate system [176]. Other studies disagree with this projection [177]. They expect R_{AA} between 2.5 and 3.5 by the end of the 21st century. CMIP6 climate models project the amplification's continued presence throughout the 21st century, with R_{AA} of about 2.4 (2 to 4 for individual models). As such, the Arctic's annual mean temperature and precipitation could reach about 11.5 ± 3.4°C and 49 ± 19% over the 2081–2100 period (with respect to a 1995–2014 baseline) under the SSP5-8.5 scenario or 4.0 ± 2.5°C and 17 ± 11% under the SSP1-2.6 scenario. It remains unclear whether the period of the most accelerated warming will be limited to the transition to a seasonally ice-free Arctic Ocean, or whether the Arctic warming pace will be still increasing in an open-water Arctic [178].

Satellite observations contribute not only to the monitoring of the amplification but also to the entire value chain that comprises data, information, knowledge, and wisdom [179]. Remote-sensing products of climate quality become integrated into body of knowledge and are used in holistic informed decision making. The ESA CCI is significant in providing data for societal benefits [180]. There is, however, more work to be done. First, more diverse long-term climate quality data products are needed. Diversification of ECV products must be complemented by studies of consistency between different products, and intercalibration should be performed if necessary. This will help to create a model-independent assessment of Arctic climate change and also of spatial and temporal scales that are still unresolved in climate models and analyses. Second, there is a need to improve the processing and cross-platform calibration of long-term climate quality data products, so that the statistical analysis of time records, specifically trends, would become more reliable. Year-round sampling capabilities and sampling of the land sea interface need to be considerably advanced. Specifically, regular atmospheric vertical profile information is still undersampled. Finally, there is a need for a standard protocol for such calibration, which would ensure the quality of long-term data sets. It is important to bring consistency to diverse data products, which at present are increasing the uncertainties of future climate projections.

Author Contributions: Conceptualization, I.E., B.S., and J.J.; methodology, I.E., B.C., L.P., and A.C.; formal analysis, I.E., L.P., A.C, and A.S.; resources, J.J. and C.D.; data curation, O.S., M.C., A.S., A.C., and I.E.; writing, I.E. and A.C.; supervision, J.J., B.S., and C.D.; project administration, J.J.; funding acquisition, J.J. and C.D. All authors have read and agreed to the published version of the manuscript.

Funding: This work was supported by the European Space Agency (contract no. 4000127401/19/NL/LF—"ARKTALAS Hoavva").

Data Availability Statement: All data sets should be requested from original references.

Conflicts of Interest: The authors declare no conflicts of interest.

References

1. Rajendran, S.; Sadooni, F.N.; Al-Kuwari, H.A.S.; Oleg, A.; Govil, H.; Nasir, S.; Vethamony, P. Monitoring Oil Spill in Norilsk, Russia Using Satellite Data. *Sci. Rep.* **2021**, *11*, 3817. https://doi.org/10.1038/s41598-021-83260-7.
2. Hjort, J.; Karjalainen, O.; Aalto, J.; Westermann, S.; Romanovsky, V.E.; Nelson, F.E.; Etzelmüller, B.; Luoto, M. Degrading Permafrost Puts Arctic Infrastructure at Risk by Mid-Century. *Nat. Commun.* **2018**, *9*, 5147. https://doi.org/10.1038/s41467-018-07557-4.
3. Hegglin, M.I.; Hollmann, R.; Ardhuin, F.; Bartsch, A.; Bastos, A.; Bennett, V.; Boutin, J.; Brockmann, C.; Buchwitz, M.; Chuvieco, E.; et al. Consistency of Satellite Climate Data Records for Earth System Monitoring. *Bull. Am. Meteorol. Soc.* **2020**, *101*, E1948–E1971. https://doi.org/10.1175/BAMS-D-19-0127.1.
4. Yang, J.; Gong, P.; Fu, R.; Zhang, M.; Chen, J.; Liang, S.; Xu, B.; Shi, J.; Dickinson, R. The Role of Satellite Remote Sensing in Climate Change Studies. *Nat. Clim. Chang.* **2013**, *3*, 875–883. https://doi.org/10.1038/nclimate1908.
5. Duncan, B.N.; Ott, L.E.; Abshire, J.B.; Brucker, L.; Carroll, M.L.; Carton, J.; Comiso, J.C.; Dinnat, E.P.; Forbes, B.C.; Gonsamo, A.; et al. Space-Based Observations for Understanding Changes in the Arctic-Boreal Zone. *Rev. Geophys.* **2020**, *58*, e2019RG000652. https://doi.org/10.1029/2019RG000652.
6. Jia, C.; Minnett, P.J. High Latitude Sea Surface Temperatures Derived from MODIS Infrared Measurements. *Remote Sens. Environ.* **2020**, *251*, 112094. https://doi.org/10.1016/j.rse.2020.112094.
7. Myers-smith, I.H.; Kerby, J.T.; Phoenix, G.K.; Bjerke, J.W.; Epstein, H.E.; Assmann, J.J.; John, C.; Andreu-hayles, L.; Angers-blondin, S.; Beck, P.S.A.; et al. Complexity Revealed in the Greening of the Arctic. *Nat. Clim. Chang.* **2020**, *10*, 106–117. https://doi.org/10.1038/s41558-019-0688-1.
8. Landrum, L.; Holland, M.M. Extremes Become Routine in an Emerging New Arctic. *Nat. Clim. Chang.* **2020**, *10*, 1108–1115. https://doi.org/10.1038/s41558-020-0892-z.
9. Taylor, P.C.; Boeke, R.C.; Boisvert, L.N.; Feldl, N.; Henry, M.; Huang, Y.; Langen, P.L.; Liu, W.; Pithan, F.; Sejas, S.A.; et al. Process Drivers, Inter-Model Spread, and the Path Forward: A Review of Amplified Arctic Warming. *Front. Earth Sci.* **2022**, *9*, 1391. https://doi.org/10.3389/feart.2021.758361.
10. Robinson, D.A.; Dewey, K.F.; Heim, R.R. Global Snow Cover Monitoring: An Update. *Bull. Am. Meteorol. Soc.* **1993**, *74*, 1689–1696. https://doi.org/10.1175/1520-0477(1993)074<1689:GSCMAU>2.0.CO;2.
11. Bojinski, S.; Verstraete, M.; Peterson, T.C.; Richter, C.; Simmons, A.; Zemp, M. The Concept of Essential Climate Variables in Support of Climate Research, Applications, and Policy. *Bull. Am. Meteorol. Soc.* **2014**, *95*, 1431–1443. https://doi.org/10.1175/BAMS-D-13-00047.1.
12. Starkweather, S.; Shapiro, H.; Vakhutinsky, S.; Druckenmiller, M. *15-Year Retrospective Analysis on AON the Observational Foundation of the Arctic Report Card—A 15-Year Retrospective Analysis on the Arctic Observing Network (AON) and Insights for the Future System*; NOAA Arctic, 2020, https://doi.org/10.25923/ahj5-z336.
13. Comiso, J.C.; Hall, D.K. Climate Trends in the Arctic as Observed from Space. *WIREs Clim. Chang.* **2014**, *5*, 389–409. https://doi.org/10.1002/wcc.277.
14. Previdi, M.; Smith, K.L.; Polvani, L.M. Arctic Amplification of Climate Change: A Review of Underlying Mechanisms. *Environ. Res. Lett.* **2021**, *16*, 093003. https://doi.org/10.1088/1748-9326/ac1c29.
15. Semenov, V.A. Modern Arctic Climate Research: Progress, Change of Concepts, and Urgent Problems. *Izv. Atmos. Ocean. Phys.* **2021**, *57*, 18–28. https://doi.org/10.1134/S0001433821010114.

16. Wendisch, M.; Brückner, M.; Crewell, S.; Ehrlich, A.; Notholt, J.; Lüpkes, C.; Macke, A.; Burrows, J.P.; Rinke, A.; Quaas, J.; et al. Atmospheric and Surface Processes, and Feedback Mechanisms Determining Arctic Amplification: A Review of First Results and Prospects of the (AC)3 Project. *Bull. Am. Meteorol. Soc.* **2022**, *104*, E208–E242. https://doi.org/10.1175/BAMS-D-21-0218.1.
17. Wang, Y.; Bi, H.; Huang, H.; Liu, Y.; Liu, Y.; Liang, X.; Fu, M.; Zhang, Z. Satellite-Observed Trends in the Arctic Sea Ice Concentration for the Period 1979–2016. *J. Oceanol. Limnol.* **2019**, *37*, 18–37. https://doi.org/10.1007/s00343-019-7284-0.
18. England, M.R.; Eisenman, I.; Lutsko, N.J.; Wagner, T.J.W. The Recent Emergence of Arctic Amplification. *Geophys. Res. Lett.* **2021**, *48*, e2021GL094086. https://doi.org/10.1029/2021GL094086.
19. Isaksen, K.; Nordli, Ø.; Ivanov, B.; Køltzow, M.A.Ø.; Aaboe, S.; Gjelten, H.M.; Mezghani, A.; Eastwood, S.; Førland, E.; Benestad, R.E.; et al. Exceptional Warming over the Barents Area. *Sci. Rep.* **2022**, *12*, 9371. https://doi.org/10.1038/s41598-022-13568-5.
20. Francis, J.A.; Vavrus, S.J. Evidence Linking Arctic Amplification to Extreme Weather in Mid-Latitude. *Geophys. Res. Lett.* **2012**, *39*, L06801. https://doi.org/10.1029/2012GL051000.
21. Johannessen, O.M.; Kuzmina, S.I.; Bobylev, L.P.; Miles, M.W. Surface Air Temperature Variability and Trends in the Arctic: New Amplification Assessment and Regionalisation. *Tellus Ser. A Dyn. Meteorol. Oceanogr.* **2016**, *68*, 28234. https://doi.org/10.3402/tellusa.v68.28234.
22. Davy, R.; Chen, L.; Hanna, E. Arctic Amplification Metrics. *Int. J. Climatol.* **2018**, *38*, 4384–4394. https://doi.org/10.1002/joc.5675.
23. Bekryaev, R.V.; Polyakov, I.V.; Alexeev, V.A. Role of Polar Amplification in Long-Term Surface Air Temperature Variations and Modern Arctic Warming. *J. Clim.* **2010**, *23*, 3888–3906. https://doi.org/10.1175/2010JCLI3297.1.
24. Nielsen-Englyst, P.; Høyer, J.L.; Kolbe, W.M.; Dybkjær, G.; Lavergne, T.; Tonboe, R.T.; Skarpalezos, S.; Karagali, I. A Combined Sea and Sea-Ice Surface Temperature Climate Dataset of the Arctic, 1982–2021. *Remote Sens. Environ.* **2023**, *284*, 113331. https://doi.org/10.1016/j.rse.2022.113331.
25. Bormann, K.J.; Brown, R.D.; Derksen, C.; Painter, T.H. Estimating Snow-Cover Trends from Space. *Nat. Clim. Chang.* **2018**, *8*, 924–928. https://doi.org/10.1038/s41558-018-0318-3.
26. Ardyna, M.; Arrigo, K.R. Phytoplankton Dynamics in a Changing Arctic Ocean. *Nat. Clim. Chang.* **2020**, *10*, 892–903. https://doi.org/10.1038/s41558-020-0905-y.
27. Nitze, I.; Grosse, G.; Jones, B.M.; Romanovsky, V.E.; Boike, J. Remote Sensing Quantifies Widespread Abundance of Permafrost Region Disturbances across the Arctic and Subarctic. *Nat. Commun.* **2018**, *9*, 5423. https://doi.org/10.1038/s41467-018-07663-3.
28. Beamish, A.; Raynolds, M.K.; Epstein, H.; Frost, G.V.; Macander, M.J.; Bergstedt, H.; Bartsch, A.; Kruse, S.; Miles, V.; Tanis, C.M.; et al. Recent Trends and Remaining Challenges for Optical Remote Sensing of Arctic Tundra Vegetation: A Review and Outlook. *Remote Sens. Environ.* **2020**, *246*, 111872. https://doi.org/10.1016/j.rse.2020.111872.
29. Trofaier, A.M.; Westermann, S.; Bartsch, A. Progress in Space-Borne Studies of Permafrost for Climate Science: Towards a Multi-ECV Approach. *Remote Sens. Environ.* **2017**, *203*, 55–70. https://doi.org/10.1016/j.rse.2017.05.021.
30. Jenkins, L.K.; Barry, T.; Bosse, K.R.; Currie, W.S.; Christensen, T.; Longan, S.; Shuchman, R.A.; Tanzer, D.; Taylor, J.J. Satellite-Based Decadal Change Assessments of Pan-Arctic Environments. *Ambio* **2020**, *49*, 820–832. https://doi.org/10.1007/s13280-019-01249-z.
31. Liang, S.; Wang, D.; He, T.; Yu, Y. Remote Sensing of Earth's Energy Budget: Synthesis and Review. *Int. J. Digit. Earth* **2019**, *12*, 737–780. https://doi.org/10.1080/17538947.2019.1597189.
32. Riihelä, A.; Key, J.R.; Meirink, J.F.; Kuipers Munneke, P.; Palo, T.; Karlsson, K.-G. An Intercomparison and Validation of Satellite-Based Surface Radiative Energy Flux Estimates over the Arctic. *J. Geophys. Res. Atmos.* **2017**, *122*, 4829–4848. https://doi.org/10.1002/2016JD026443.
33. Wang, X.; Key, J.; Liu, Y.; Fowler, C.; Maslanik, J.; Tschudi, M. Arctic Climate Variability and Trends from Satellite Observations. *Adv. Meteorol.* **2012**, *2012*, 505613. https://doi.org/10.1155/2012/505613.
34. Rantanen, M.; Karpechko, A.Y.; Lipponen, A.; Nordling, K.; Hyvärinen, O.; Ruosteenoja, K.; Vihma, T.; Laaksonen, A. The Arctic Has Warmed Nearly Four Times Faster than the Globe since 1979. *Commun. Earth Environ.* **2022**, *3*, 168. https://doi.org/10.1038/s43247-022-00498-3.
35. Lind, S.; Ingvaldsen, R.B.; Furevik, T. Arctic warming hotspot in the northern Barents Sea linked to declining sea-ice import. *Nat. Clim. Chang.* **2018**, *8*, 634–639. https://doi.org/10.1038/s41558-018-0205-y.
36. Ricker, R.; Kauker, F.; Schweiger, A.; Hendricks, S.; Zhang, J.; Paul, S. Evidence for an Increasing Role of Ocean Heat in Arctic Winter Sea Ice Growth. *J. Clim.* **2021**, *34*, 5215–5227. https://doi.org/10.1175/JCLI-D-20-0848.1.
37. Yang, X.-Y.; Fyfe, J.C.; Flato, G.M. The Role of Poleward Energy Transport in Arctic Temperature Evolution. *Geophys. Res. Lett.* **2010**, *37*. https://doi.org/10.1029/2010GL043934.
38. Liu, Y.; Key, J.R.; Schweiger, A.; Francis, J. Characteristics of Satellite-Derived Clear-Sky Atmospheric Temperature Inversion Strength in the Arctic, 1980–1996. *J. Clim.* **2006**, *19*, 4902–4913. https://doi.org/10.1175/JCLI3915.1.
39. Sobrino, J.A.; Julien, Y.; García-Monteiro, S. Surface Temperature of the Planet Earth from Satellite Data. *Remote Sens.* **2020**, *12*, 218. https://doi.org/10.3390/rs12020218.
40. Wang, Y.; Hessen, D.O.; Samset, B.H.; Stordal, F. Evaluating Global and Regional Land Warming Trends in the Past Decades with Both MODIS and ERA5-Land Land Surface Temperature Data. *Remote Sens. Environ.* **2022**, *280*, 113181. https://doi.org/10.1016/j.rse.2022.113181.
41. Li, M.; Ke, C.Q.; Shen, X.; Cheng, B.; Li, H. Investigation of the Arctic Sea Ice Volume from 2002 to 2018 Using Multi-Source Data. *Int. J. Climatol.* **2021**, *41*, 2509–2527. https://doi.org/10.1002/joc.6972.

42. Bi, H.; Liang, Y.; Wang, Y.; Liang, X.; Zhang, Z.; Du, T.; Yu, Q.; Huang, J.; Kong, M.; Huang, H. Arctic Multiyear Sea Ice Variability Observed from Satellites: A Review. *J. Oceanol. Limnol.* **2020**, *38*, 962–984. https://doi.org/10.1007/s00343-020-0093-7.
43. Liu, Y.; Key, J.R.; Wang, X.; Tschudi, M. Multidecadal Arctic Sea Ice Thickness and Volume Derived from Ice Age. *Cryosph.* **2020**, *14*, 1325–1345. https://doi.org/10.5194/tc-14-1325-2020.
44. Kwok, R. Arctic Sea Ice Thickness, Volume, and Multiyear Ice Coverage: Losses and Coupled Variability (1958-2018). *Environ. Res. Lett.* **2018**, *13*, 105005. https://doi.org/10.1088/1748-9326/aae3ec.
45. Feng, J.; Zhang, Y.; Cheng, Q.; Tsou, J.Y. Pan-Arctic Melt Pond Fraction Trend, Variability, and Contribution to Sea Ice Changes. *Glob. Planet. Chang.* **2022**, *217*, 103932. https://doi.org/10.1016/j.gloplacha.2022.103932.
46. Pulliainen, J.; Luojus, K.; Derksen, C.; Mudryk, L.; Lemmetyinen, J.; Salminen, M.; Ikonen, J.; Takala, M.; Cohen, J.; Smolander, T.; et al. Patterns and Trends of Northern Hemisphere Snow Mass from 1980 to 2018. *Nature* **2020**, *581*, 294–298. https://doi.org/10.1038/s41586-020-2258-0.
47. Devasthale, A.; Sedlar, J.; Tjernström, M.; Kokhanovsky, A. A Climatological Overview of Arctic Clouds. In *Physics and Chemistry of the Arctic Atmosphere*; Springer: Cham, Switzerland, 2020; pp. 331–360.
48. Hwang, J.; Choi, Y.; Su, H.; Jiang, J.H. Invariability of Arctic Top-of-Atmosphere Radiative Response to Surface Temperature Changes. *Earth Space Sci.* **2020**, *7*, e2020EA001316. https://doi.org/10.1029/2020EA001316.
49. Riihelä, A.; Manninen, T.; Laine, V. Observed Changes in the Albedo of the Arctic Sea-Ice Zone for the Period 1982–2009. *Nat. Clim. Chang.* **2013**, *3*, 895–898. https://doi.org/10.1038/nclimate1963.
50. Pistone, K.; Eisenman, I.; Ramanathan, V. Observational Determination of Albedo Decrease Caused by Vanishing Arctic Sea Ice. *Proc. Natl. Acad. Sci. USA* **2014**, *111*, 3322–3326. https://doi.org/10.1073/pnas.1318201111.
51. Marcianesi, F.; Aulicino, G.; Wadhams, P. Arctic Sea Ice and Snow Cover Albedo Variability and Trends during the Last Three Decades. *Polar Sci.* **2021**, *28*, 100617. https://doi.org/10.1016/j.polar.2020.100617.
52. Seong, N.; Kim, H.-C.; Choi, S.; Jin, D.; Jung, D.; Sim, S.; Woo, J.; Kim, N.; Seo, M.; Lee, K.; et al. Evaluation of Sea Ice Radiative Forcing According to Surface Albedo and Skin Temperature over the Arctic from 1982–2015. *Remote Sens.* **2022**, *14*, 2512. https://doi.org/10.3390/rs14112512.
53. Cao, Y.; Liang, S.; Chen, X.; He, T. Assessment of Sea Ice Albedo Radiative Forcing and Feedback over the Northern Hemisphere from 1982 to 2009 Using Satellite and Reanalysis Data. *J. Clim.* **2015**, *28*, 1248–1259. https://doi.org/10.1175/JCLI-D-14-00389.1.
54. Park, H.; Kim, Y.; Kimball, J.S. Widespread Permafrost Vulnerability and Soil Active Layer Increases over the High Northern Latitudes Inferred from Satellite Remote Sensing and Process Model Assessments. *Remote Sens. Environ.* **2016**, *175*, 349–358. https://doi.org/10.1016/j.rse.2015.12.046.
55. Philipp, M.; Dietz, A.; Buchelt, S.; Kuenzer, C. Trends in Satellite Earth Observation for Permafrost Related Analyses-a Review. *Remote Sens.* **2021**, *13*, 1217. https://doi.org/10.3390/rs13061217.
56. Obu, J.; Westermann, S.; Bartsch, A.; Berdnikov, N.; Christiansen, H.H.; Dashtseren, A.; Delaloye, R.; Elberling, B.; Etzelmüller, B.; Kholodov, A.; et al. Northern Hemisphere Permafrost Map Based on TTOP Modelling for 2000–2016 at 1 Km2 Scale. *Earth-Sci. Rev.* **2019**, *193*, 299–316. https://doi.org/10.1016/j.earscirev.2019.04.023.
57. Park, T.; Ganguly, S.; Tømmervik, H.; Euskirchen, E.S.; Høgda, K.-A.; Karlsen, S.R.; Brovkin, V.; Nemani, R.R.; Myneni, R.B. Changes in Growing Season Duration and Productivity of Northern Vegetation Inferred from Long-Term Remote Sensing Data. *Environ. Res. Lett.* **2016**, *11*, 084001. https://doi.org/10.1088/1748-9326/11/8/084001.
58. The IMBIE team Mass Balance of the Greenland Ice Sheet from 1992 to 2018. *Nature* **2020**, *579*, 233–239. https://doi.org/10.1038/s41586-019-1855-2.
59. Mottram, R.; Simonsen, S.B.; Høyer Svendsen, S.; Barletta, V.R.; Sandberg Sørensen, L.; Nagler, T.; Wuite, J.; Groh, A.; Horwath, M.; Rosier, J.; et al. An Integrated View of Greenland Ice Sheet Mass Changes Based on Models and Satellite Observations. *Remote Sens.* **2019**, *11*, 1407. https://doi.org/10.3390/rs11121407.
60. Cooper, M.; Smith, L. Satellite Remote Sensing of the Greenland Ice Sheet Ablation Zone: A Review. *Remote Sens.* **2019**, *11*, 2405. https://doi.org/10.3390/rs11202405.
61. Bartsch, A.; Pointner, G.; Nitze, I.; Efimova, A.; Jakober, D.; Ley, S.; Högström, E.; Grosse, G.; Schweitzer, P. Expanding Infrastructure and Growing Anthropogenic Impacts along Arctic Coasts. *Environ. Res. Lett.* **2021**, *16*, 115013. https://doi.org/10.1088/1748-9326/ac3176.
62. Bartsch, A.; Pointner, G.; Ingeman-Nielsen, T.; Lu, W. Towards Circumpolar Mapping of Arctic Settlements and Infrastructure Based on Sentinel-1 and Sentinel-2. *Remote Sens.* **2020**, *12*, 2368. https://doi.org/10.3390/RS12152368.
63. Sasgen, I.; Wouters, B.; Gardner, A.S.; King, M.D.; Tedesco, M.; Landerer, F.W.; Dahle, C.; Save, H.; Fettweis, X. Return to Rapid Ice Loss in Greenland and Record Loss in 2019 Detected by the GRACE-FO Satellites. *Commun. Earth Environ.* **2020**, *1*, 8. https://doi.org/10.1038/s43247-020-0010-1.
64. Spencer, R.W.; Christy, J.R.; Braswell, W.D. UAH Version 6 Global Satellite Temperature Products: Methodology and Results. *Asia-Pac. J. Atmos. Sci.* **2017**, *53*, 121–130. https://doi.org/10.1007/s13143-017-0010-y.
65. Christy, J.R.; Spencer, R.W.; Braswell, W.D.; Doty, K.G.; NOAA CDR Program. *NOAA Climate Data Record (CDR) of MSU and AMSU-A Mean Layer Temperatures, UAH Version 6.0*; NOAA National Centers for Environmental Information. 2017, https://doi.org/10.7289/V5MC8X31 [access date 11.11.2022].
66. Guay, K.C.; Beck, P.S.A.; Berner, L.T.; Goetz, S.J.; Baccini, A.; Buermann, W. Vegetation Productivity Patterns at High Northern Latitudes: A Multi-Sensor Satellite Data Assessment. *Glob. Chang. Biol.* **2014**, *20*, 3147–3158. https://doi.org/10.1111/gcb.12647.

67. Lancheros, E.; Camps, A.; Park, H.; Sicard, P.; Mangin, A.; Matevosyan, H.; Lluch, I. Gaps Analysis and Requirements Specification for the Evolution of Copernicus System for Polar Regions Monitoring: Addressing the Challenges in the Horizon 2020–2030. *Remote Sens.* **2018**, *10*, 1098. https://doi.org/10.3390/rs10071098.
68. Hollmann, R.; Merchant, C.J.; Saunders, R.; Downy, C.; Buchwitz, M.; Cazenave, A.; Chuvieco, E.; Defourny, P.; de Leeuw, G.; Forsberg, R.; et al. The ESA Climate Change Initiative: Satellite Data Records for Essential Climate Variables. *Bull. Am. Meteorol. Soc.* **2013**, *94*, 1541–1552. https://doi.org/10.1175/BAMS-D-11-00254.1.
69. Nightingale, J.; Boersma, K.; Muller, J.-P.; Compernolle, S.; Lambert, J.-C.; Blessing, S.; Giering, R.; Gobron, N.; De Smedt, I.; Coheur, P.; et al. Quality Assurance Framework Development Based on Six New ECV Data Products to Enhance User Confidence for Climate Applications. *Remote Sens.* **2018**, *10*, 1254. https://doi.org/10.3390/rs10081254.
70. Kharbouche, S.; Muller, J.-P. Sea Ice Albedo from MISR and MODIS: Production, Validation, and Trend Analysis. *Remote Sens.* **2018**, *11*, 9. https://doi.org/10.3390/rs11010009.
71. Bentamy, A.; Piollé, J.F.; Grouazel, A.; Danielson, R.; Gulev, S.; Paul, F.; Azelmat, H.; Mathieu, P.P.; von Schuckmann, K.; Sathyendranath, S.; et al. Review and Assessment of Latent and Sensible Heat Flux Accuracy over the Global Oceans. *Remote Sens. Environ.* **2017**, *201*, 196–218. https://doi.org/10.1016/j.rse.2017.08.016.
72. Smedsrud, L.H.; Esau, I.; Ingvaldsen, R.B.; Eldevik, T.; Haugan, P.M.; Li, C.; Lien, V.S.; Olsen, A.; Omar, A.M.; Otterå, O.H.; et al. The role of the barents sea in the arctic climate system. *Rev. Geophys.* **2013**, *51*, 415–449. https://doi.org/10.1002/rog.20017.
73. Santer, B.D.; Solomon, S.; Pallotta, G.; Mears, C.; Po-Chedley, S.; Fu, Q.; Wentz, F.; Zou, C.Z.; Painter, J.; Cvijanovic, I.; et al. Comparing Tropospheric Warming in Climate Models and Satellite Data. *J. Clim.* **2017**, *30*, 373–392. https://doi.org/10.1175/JCLI-D-16-0333.1.
74. Karlsson, K.-G.; Anttila, K.; Trentmann, J.; Stengel, M.; Fokke Meirink, J.; Devasthale, A.; Hanschmann, T.; Kothe, S.; Jääskeläinen, E.; Sedlar, J.; et al. CLARA-A2: The Second Edition of the CM SAF Cloud and Radiation Data Record from 34 Years of Global AVHRR Data. *Atmos. Chem. Phys.* **2017**, *17*, 5809–5828. https://doi.org/10.5194/acp-17-5809-2017.
75. Loeb, N.G.; Doelling, D.R.; Wang, H.; Su, W.; Nguyen, C.; Corbett, J.G.; Liang, L.; Mitrescu, C.; Rose, F.G.; Kato, S. Clouds and the Earth's Radiant Energy System (CERES) Energy Balanced and Filled (EBAF) Top-of-Atmosphere (TOA) Edition-4.0 Data Product. *J. Clim.* **2018**, *31*, 895–918. https://doi.org/10.1175/JCLI-D-17-0208.1.
76. Heidinger, A.K.; Foster, M.J.; Walther, A.; Zhao, X. (Tom) The Pathfinder Atmospheres–Extended AVHRR Climate Dataset. *Bull. Am. Meteorol. Soc.* **2014**, *95*, 909–922. https://doi.org/10.1175/BAMS-D-12-00246.1.
77. Wang, X.; Key, J.R. Arctic Surface, Cloud, and Radiation Properties Based on the AVHRR Polar Pathfinder Dataset. Part II: Recent Trends. *J. Clim.* **2005**, *18*, 2575–2593. https://doi.org/10.1175/JCLI3439.1.
78. Wang, X.; Liu, J.; Yang, B.; Bao, Y.; Petropoulos, G.P.; Liu, H.; Hu, B. Seasonal Trends in Clouds and Radiation over the Arctic Seas from Satellite Observations during 1982 to 2019. *Remote Sens.* **2021**, *13*, 3201. https://doi.org/10.3390/rs13163201.
79. Estilow, T.W.; Young, A.H.; Robinson, D.A. A Long-Term Northern Hemisphere Snow Cover Extent Data Record for Climate Studies and Monitoring. *Earth Syst. Sci. Data* **2015**, *7*, 137–142. https://doi.org/10.5194/essd-7-137-2015.
80. Lavergne, T.; Macdonald Sørensen, A.; Kern, S.; Tonboe, R.; Notz, D.; Aaboe, S.; Bell, L.; Dybkjær, G.; Eastwood, S.; Gabarro, C.; et al. Version 2 of the EUMETSAT OSI SAF and ESA CCI Sea-Ice Concentration Climate Data Records. *Cryosphere* **2019**, *13*, 49–78. https://doi.org/10.5194/tc-13-49-2019.
81. Comiso, J.C.; Meier, W.N.; Gersten, R. Variability and Trends in the Arctic Sea Ice Cover: Results from Different Techniques. *J. Geophys. Res. Ocean.* **2017**, *122*, 6883–6900. https://doi.org/10.1002/2017JC012768.
82. Schweiger, A.J.; Wood, K.R.; Zhang, J. Arctic Sea Ice Volume Variability over 1901–2010: A Model-Based Reconstruction. *J. Clim.* **2019**, *32*, 4731–4752. https://doi.org/10.1175/JCLI-D-19-0008.1.
83. Piao, S.; Wang, X.; Park, T.; Chen, C.; Lian, X.; He, Y.; Bjerke, J.W.; Chen, A.; Ciais, P.; Tømmervik, H.; et al. Characteristics, Drivers and Feedbacks of Global Greening. *Nat. Rev. Earth Environ.* **2020**, *1*, 14–27. https://doi.org/10.1038/s43017-019-0001-x.
84. Pinzon, J.; Tucker, C. A Non-Stationary 1981–2012 AVHRR NDVI3g Time Series. *Remote Sens.* **2014**, *6*, 6929–6960. https://doi.org/10.3390/rs6086929.
85. Kim, Y.; Kimball, J.S.; Glassy, J.; Du, J. An Extended Global Earth System Data Record on Daily Landscape Freeze–Thaw Status Determined from Satellite Passive Microwave Remote Sensing. *Earth Syst. Sci. Data* **2017**, *9*, 133–147. https://doi.org/10.5194/essd-9-133-2017.
86. Holland, M.M.; Bitz, C.M. Polar Amplification of Climate Change in Coupled Models. *Clim. Dyn.* **2003**, *21*, 221–232. https://doi.org/10.1007/s00382-003-0332-6.
87. Serreze, M.C.; Barry, R.G. Processes and Impacts of Arctic Amplification: A Research Synthesis. *Glob. Planet. Chang.* **2011**, *77*, 85–96. https://doi.org/10.1016/j.gloplacha.2011.03.004.
88. Comiso, J.C. Warming Trends in the Arctic from Clear Sky Satellite Observations. *J. Clim.* **2003**, *16*, 3498–3510. https://doi.org/10.1175/1520-0442(2003)016<3498:WTITAF>2.0.CO;2.
89. Serreze, M.C.; Francis, J.A. The Arctic Amplification Debate. *Clim. Chang.* **2006**, *76*, 241–264. https://doi.org/10.1007/s10584-005-9017-y.
90. Box, J.E.; Colgan, W.T.; Christensen, T.R.; Schmidt, N.M.; Lund, M.; Parmentier, F.J.W.; Brown, R.; Bhatt, U.S.; Euskirchen, E.S.; Romanovsky, V.E.; et al. Key Indicators of Arctic Climate Change: 1971-2017. *Environ. Res. Lett.* **2019**, *14*, 45010. https://doi.org/10.1088/1748-9326/aafc1b.
91. Screen, J.A.; Deser, C.; Simmonds, I. Local and Remote Controls on Observed Arctic Warming. *Geophys. Res. Lett.* **2012**, *39*. https://doi.org/10.1029/2012GL051598.

92. Babar, B.; Graversen, R.; Boström, T. Evaluating CM-SAF Solar Radiation CLARA-A1 and CLARA-A2 Datasets in Scandinavia. *Sol. Energy* **2018**, *170*, 76–85. https://doi.org/10.1016/j.solener.2018.05.009.
93. Lohmann, G. Temperatures from Energy Balance Models: The Effective Heat Capacity Matters. *Earth Syst. Dyn.* **2020**, *11*, 1195–1208. https://doi.org/10.5194/esd-11-1195-2020.
94. Mayer, M.; Tietsche, S.; Haimberger, L.; Tsubouchi, T.; Mayer, J.; Zuo, H. An Improved Estimate of the Coupled Arctic Energy Budget. *J. Clim.* **2019**, *32*, 7915–7934. https://doi.org/10.1175/JCLI-D-19-0233.1.
95. Jeevanjee, N.; Held, I.; Ramaswamy, V. Manabe's Radiative–Convective Equilibrium. *Bull. Am. Meteorol. Soc.* **2022**, *103*, E2559–E2569. https://doi.org/10.1175/BAMS-D-21-0351.1.
96. Thackeray, C.W.; Hall, A. An Emergent Constraint on Future Arctic Sea-Ice Albedo Feedback. *Nat. Clim. Chang.* **2019**, *9*, 972–978. https://doi.org/10.1038/s41558-019-0619-1.
97. Olonscheck, D.; Mauritsen, T.; Notz, D. Arctic Sea-Ice Variability Is Primarily Driven by Atmospheric Temperature Fluctuations. *Nat. Geosci.* **2019**, *12*, 430–434. https://doi.org/10.1038/s41561-019-0363-1.
98. Bliss, A.C.; Anderson, M.R. Arctic Sea Ice Melt Onset Timing From Passive Microwave-Based and Surface Air Temperature-Based Methods. *J. Geophys. Res. Atmos.* **2018**, *123*, 9063–9080. https://doi.org/10.1029/2018JD028676.
99. Bitz, C.M.; Roe, G.H. A Mechanism for the High Rate of Sea Ice Thinning in the Arctic Ocean. *J. Clim.* **2004**, *17*, 3623–3632. https://doi.org/10.1175/1520-0442(2004)017<3623:AMFTHR>2.0.CO;2.
100. Brennan, M.K.; Hakim, G.J.; Blanchard-Wrigglesworth, E. Arctic Sea-Ice Variability During the Instrumental Era. *Geophys. Res. Lett.* **2020**, *47*, e2019GL086843. https://doi.org/10.1029/2019GL086843.
101. Serreze, M.C.; Barrett, A.P.; Stroeve, J.C.; Kindig, D.N.; Holland, M.M. The Emergence of Surface-Based Arctic Amplification. *Cryosphere* **2009**, *3*, 11–19. https://doi.org/10.5194/tc-3-11-2009.
102. Johannessen, O.M.; Bobylev, L.P.; Shalina, E.V.; Sandven, S. (Eds.) *Sea Ice in the Arctic*; Springer Polar Sciences; Springer International Publishing: Cham, Switzerland, 2020; ISBN 978-3-030-21300-8.
103. Ivanova, N.; Pedersen, L.T.; Tonboe, R.T.; Kern, S.; Heygster, G.; Lavergne, T.; Sørensen, A.; Saldo, R.; Dybkjær, G.; Brucker, L.; et al. Inter-Comparison and Evaluation of Sea Ice Algorithms: Towards Further Identification of Challenges and Optimal Approach Using Passive Microwave Observations. *Cryosphere* **2015**, *9*, 1797–1817. https://doi.org/10.5194/tc-9-1797-2015.
104. Ólason, E.; Rampal, P.; Dansereau, V. On the Statistical Properties of Sea-Ice Lead Fraction and Heat Fluxes in the Arctic. *Cryosphere* **2021**, *15*, 1053–1064. https://doi.org/10.5194/tc-15-1053-2021.
105. Zhang, Y.; Cheng, X.; Liu, J.; Hui, F. The Potential of Sea Ice Leads as a Predictor for Summer Arctic Sea Ice Extent. *Cryosphere* **2018**, *12*, 3747–3757. https://doi.org/10.5194/tc-12-3747-2018.
106. Wagner, P.M.; Hughes, N.; Bourbonnais, P.; Stroeve, J.; Rabenstein, L.; Bhatt, U.; Little, J.; Wiggins, H.; Fleming, A. Sea-Ice Information and Forecast Needs for Industry Maritime Stakeholders. *Polar Geogr.* **2020**, *43*, 160–187. https://doi.org/10.1080/1088937X.2020.1766592.
107. Marquardt Collow, A.B.; Cullather, R.I.; Bosilovich, M.G. Recent Arctic Ocean Surface Air Temperatures in Atmospheric Reanalyses and Numerical Simulations. *J. Clim.* **2020**, *33*, 4347–4367. https://doi.org/10.1175/JCLI-D-19-0703.1.
108. Minnett, P.J.; Alvera-Azcárate, A.; Chin, T.M.; Corlett, G.K.; Gentemann, C.L.; Karagali, I.; Li, X.; Marsouin, A.; Marullo, S.; Maturi, E.; et al. Half a Century of Satellite Remote Sensing of Sea-Surface Temperature. *Remote Sens. Environ.* **2019**, *233*, 111366. https://doi.org/10.1016/j.rse.2019.111366.
109. Kumar, A.; Yadav, J.; Mohan, R. Spatio-Temporal Change and Variability of Barents-Kara Sea Ice, in the Arctic: Ocean and Atmospheric Implications. *Sci. Total Environ.* **2021**, *753*, 142046. https://doi.org/10.1016/j.scitotenv.2020.142046.
110. Lang, A.; Yang, S.; Kaas, E. Sea Ice Thickness and Recent Arctic Warming. *Geophys. Res. Lett.* **2017**, *44*, 409–418. https://doi.org/10.1002/2016GL071274.
111. Chemke, R.; Polvani, L.M.; Kay, J.E.; Orbe, C. Quantifying the Role of Ocean Coupling in Arctic Amplification and Sea-Ice Loss over the 21st Century. *NPJ Clim. Atmos. Sci.* **2021**, *4*, 46. https://doi.org/10.1038/s41612-021-00204-8.
112. Tschudi, M.; Meier, W.N.; Stewart, J.S.; Fowler, C.; Maslanik, J. *EASE-Grid Sea Ice Age, Version 4 [Data Set]*; NASA National Snow and Ice Data Center Distributed Active Archive Center: Boulder, CO, USA, 2019.
113. Matveeva, T.A.; Semenov, V.A. Regional Features of the Arctic Sea Ice Area Changes in 2000–2019 versus 1979–1999 Periods. *Atmosphere* **2022**, *13*, 1434. https://doi.org/10.3390/atmos13091434.
114. Philipp, D.; Stengel, M.; Ahrens, B. Analyzing the Arctic Feedback Mechanism between Sea Ice and Low-Level Clouds Using 34 Years of Satellite Observations. *J. Clim.* **2020**, *33*, 7479–7501. https://doi.org/10.1175/JCLI-D-19-0895.1.
115. Luo, T.; Yuan, R.; Wang, Z. Lidar-Based Remote Sensing of Atmospheric Boundary Layer Height over Land and Ocean. *Atmos. Meas. Tech.* **2014**, *7*, 173–182. https://doi.org/10.5194/amt-7-173-2014.
116. Dang, R.; Yang, Y.; Hu, X.M.; Wang, Z.; Zhang, S. A Review of Techniques for Diagnosing the Atmospheric Boundary Layer Height (ABLH) Using Aerosol Lidar Data. *Remote Sens.* **2019**, *11*, 1590. https://doi.org/10.3390/rs11131590.
117. McGrath-Spangler, E.L.; Denning, A.S. Global Seasonal Variations of Midday Planetary Boundary Layer Depth from CALIPSO Space-Borne LIDAR. *J. Geophys. Res. Atmos.* **2013**, *118*, 1226–1233. https://doi.org/10.1002/jgrd.50198.
118. Kim, M.-H.; Yeo, H.; Park, S.; Park, D.-H.; Omar, A.; Nishizawa, T.; Shimizu, A.; Kim, S.-W. Assessing CALIOP-Derived Planetary Boundary Layer Height Using Ground-Based Lidar. *Remote Sens.* **2021**, *13*, 1496. https://doi.org/10.3390/rs13081496.
119. Von Engeln, A.; Teixeira, J. A Planetary Boundary Layer Height Climatology Derived from ECMWF Reanalysis Data. *J. Clim.* **2013**, *26*, 6575–6590. https://doi.org/10.1175/JCLI-D-12-00385.1.

120. Ao, C.O.; Waliser, D.E.; Chan, S.K.; Li, J.L.; Tian, B.; Xie, F.; Mannucci, A.J. Planetary Boundary Layer Heights from GPS Radio Occultation Refractivity and Humidity Profiles. *J. Geophys. Res. Atmos.* **2012**, *117*, 1–18. https://doi.org/10.1029/2012JD017598.
121. Ganeshan, M.; Wu, D.L. An Investigation of the Arctic Inversion Using COSMIC RO Observations. *J. Geophys. Res. Atmos.* **2015**, *120*, 9338–9351. https://doi.org/10.1002/2015JD023058.
122. Ding, F.; Iredell, L.; Theobald, M.; Wei, J.; Meyer, D. PBL Height From AIRS, GPS RO, and MERRA-2 Products in NASA GES DISC and Their 10-Year Seasonal Mean Intercomparison. *Earth Space Sci.* **2021**, *8*, e2021EA001859. https://doi.org/10.1029/2021EA001859.
123. Esau, I.N. Amplification of Turbulent Exchange over Wide Arctic Leads: Large-Eddy Simulation Study. *J. Geophys. Res. Atmos.* **2007**, *112*. D08109, https://doi.org/10.1029/2006JD007225.
124. Qu, M.; Pang, X.; Zhao, X.; Zhang, J.; Ji, Q.; Fan, P. Estimation of Turbulent Heat Flux over Leads Using Satellite Thermal Images. *Cryosph.* **2019**, *13*, 1565–1582. https://doi.org/10.5194/tc-13-1565-2019.
125. Chernokulsky, A.; Esau, I. Cloud Cover and Cloud Types in the Eurasian Arctic in 1936–2012. *Int. J. Climatol.* **2019**, *39*, 5771–5790. https://doi.org/10.1002/joc.6187.
126. Lenaerts, J.T.M.; Van Tricht, K.; Lhermitte, S.; L'Ecuyer, T.S. Polar Clouds and Radiation in Satellite Observations, Reanalyses, and Climate Models. *Geophys. Res. Lett.* **2017**, *44*, 3355–3364. https://doi.org/10.1002/2016GL072242.
127. Karlsson, K.-G.; Devasthale, A. Inter-Comparison and Evaluation of the Four Longest Satellite-Derived Cloud Climate Data Records: CLARA-A2, ESA Cloud CCI V3, ISCCP-HGM, and PATMOS-X. *Remote Sens.* **2018**, *10*, 1567. https://doi.org/10.3390/rs10101567.
128. Stengel, M.; Stapelberg, S.; Sus, O.; Schlundt, C.; Poulsen, C.; Thomas, G.; Christensen, M.; Carbajal Henken, C.; Preusker, R.; Fischer, J.; et al. Cloud Property Datasets Retrieved from AVHRR, MODIS, AATSR and MERIS in the Framework of the Cloud_cci Project. *Earth Syst. Sci. Data* **2017**, *9*, 881–904. https://doi.org/10.5194/essd-9-881-2017.
129. Stengel, M.; Stapelberg, S.; Sus, O.; Finkensieper, S.; Würzler, B.; Philipp, D.; Hollmann, R.; Poulsen, C.; Christensen, M.; McGarragh, G. Cloud_cci Advanced Very High Resolution Radiometer Post Meridiem (AVHRR-PM) Dataset Version 3: 35-Year Climatology of Global Cloud and Radiation Properties. *Earth Syst. Sci. Data* **2020**, *12*, 41–60. https://doi.org/10.5194/essd-12-41-2020.
130. Chernokulsky, A.; Mokhov, I.I. Climatology of Total Cloudiness in the Arctic: An Intercomparison of Observations and Reanalyses. *Adv. Meteorol.* **2012**, *2012*, 542093. https://doi.org/10.1155/2012/542093.
131. Chan, M.A.; Comiso, J.C. Arctic Cloud Characteristics as Derived from MODIS, CALIPSO, and CloudSat. *J. Clim.* **2013**, *26*, 3285–3306. https://doi.org/10.1175/JCLI-D-12-00204.1.
132. Liu, Y.; Ackerman, S.A.; Maddux, B.C.; Key, J.R.; Frey, R.A. Errors in Cloud Detection over the Arctic Using a Satellite Imager and Implications for Observing Feedback Mechanisms. *J. Clim.* **2010**, *23*, 1894–1907. https://doi.org/10.1175/2009JCLI3386.1.
133. Boccolari, M.; Parmiggiani, F. Trends and Variability of Cloud Fraction Cover in the Arctic, 1982–2009. *Theor. Appl. Climatol.* **2018**, *132*, 739–749. https://doi.org/10.1007/s00704-017-2125-6.
134. Hwang, J.; Choi, Y.S.; Kim, W.M.; Su, H.; Jiang, J.H. Observational Estimation of Radiative Feedback to Surface Air Temperature over Northern High Latitudes. *Clim. Dyn.* **2018**, *50*, 615–628. https://doi.org/10.1007/s00382-017-3629-6.
135. Zhang, R.; Wang, H.; Fu, Q.; Pendergrass, A.G.; Wang, M.; Yang, Y.; Ma, P.; Rasch, P.J. Local Radiative Feedbacks Over the Arctic Based on Observed Short-Term Climate Variations. *Geophys. Res. Lett.* **2018**, *45*, 5761–5770. https://doi.org/10.1029/2018GL077852.
136. Kay, J.E.; L'Ecuyer, T. Observational Constraints on Arctic Ocean Clouds and Radiative Fluxes during the Early 21st Century. *J. Geophys. Res. Atmos.* **2013**, *118*, 7219–7236. https://doi.org/10.1002/jgrd.50489.
137. Kay, J.E.; L'Ecuyer, T.; Chepfer, H.; Loeb, N.; Morrison, A.; Cesana, G. Recent Advances in Arctic Cloud and Climate Research. *Curr. Clim. Chang. Rep.* **2016**, *2*, 159–169. https://doi.org/10.1007/s40641-016-0051-9.
138. Pithan, F.; Mauritsen, T. Arctic Amplification Dominated by Temperature Feedbacks in Contemporary Climate Models. *Nat. Geosci.* **2014**, *7*, 181–184. https://doi.org/10.1038/ngeo2071.
139. Palm, S.P.; Strey, S.T.; Spinhirne, J.; Markus, T. Influence of Arctic Sea Ice Extent on Polar Cloud Fraction and Vertical Structure and Implications for Regional Climate. *J. Geophys. Res.* **2010**, *115*, D21209. https://doi.org/10.1029/2010JD013900.
140. Goosse, H.; Kay, J.E.; Armour, K.C.; Bodas-Salcedo, A.; Chepfer, H.; Docquier, D.; Jonko, A.; Kushner, P.J.; Lecomte, O.; Massonnet, F.; et al. Quantifying Climate Feedbacks in Polar Regions. *Nat. Commun.* **2018**, *9*, 1919. https://doi.org/10.1038/s41467-018-04173-0.
141. Terai, C.R.; Klein, S.A.; Zelinka, M.D. Constraining the Low-Cloud Optical Depth Feedback at Middle and High Latitudes Using Satellite Observations. *J. Geophys. Res. Atmos.* **2016**, *121*, 9696–9716. https://doi.org/10.1002/2016JD025233.
142. Sledd, A.; L'Ecuyer, T. How Much Do Clouds Mask the Impacts of Arctic Sea Ice and Snow Cover Variations? Different Perspectives from Observations and Reanalyses. *Atmosphere* **2019**, *10*, 12. https://doi.org/10.3390/atmos10010012.
143. Zhang, R.; Wang, H.; Fu, Q.; Rasch, P.J.; Wang, X. Unraveling Driving Forces Explaining Significant Reduction in Satellite-Inferred Arctic Surface Albedo since the 1980s. *Proc. Natl. Acad. Sci. USA* **2019**, *116*, 23947–23953. https://doi.org/10.1073/pnas.1915258116.
144. Walsh, J.E.; Ballinger, T.J.; Euskirchen, E.S.; Hanna, E.; Mård, J.; Overland, J.E.; Tangen, H.; Vihma, T. Extreme Weather and Climate Events in Northern Areas: A Review. *Earth-Science Rev.* **2020**, *209*, 103324. https://doi.org/10.1016/j.earscirev.2020.103324.

145. Dobricic, S.; Russo, S.; Pozzoli, L.; Wilson, J.; Vignati, E. Increasing Occurrence of Heat Waves in the Terrestrial Arctic. *Environ. Res. Lett.* **2020**, *15*, 024022. https://doi.org/10.1088/1748-9326/ab6398.
146. Vincent, W.F. Arctic Climate Change: Local Impacts, Global Consequences, and Policy Implications. In *The Palgrave Handbook of Arctic Policy and Politics*; Springer International Publishing: Cham, Switzerland, 2020; pp. 507–526.
147. Smith, D.M.; Eade, R.; Andrews, M.B.; Ayres, H.; Clark, A.; Chripko, S.; Deser, C.; Dunstone, N.J.; García-Serrano, J.; Gastineau, G.; et al. Robust but Weak Winter Atmospheric Circulation Response to Future Arctic Sea Ice Loss. *Nat. Commun.* **2022**, *13*, 727. https://doi.org/10.1038/s41467-022-28283-y.
148. Cohen, J.; Zhang, X.; Francis, J.; Jung, T.; Kwok, R.; Overland, J.; Ballinger, T.J.; Bhatt, U.S.; Chen, H.W.; Coumou, D.; et al. Divergent Consensuses on Arctic Amplification Influence on Midlatitude Severe Winter Weather. *Nat. Clim. Chang.* **2020**, *10*, 20–29.https://doi.org/10.1038/s41558-019-0662-y.
149. Alkama, R.; Koffi, E.N.; Vavrus, S.J.; Diehl, T.; Francis, J.A.; Stroeve, J.; Forzieri, G.; Vihma, T.; Cescatti, A. Wind Amplifies the Polar Sea Ice Retreat. *Environ. Res. Lett.* **2020**, *15*, 124022. https://doi.org/10.1088/1748-9326/abc379.
150. Blackport, R.; Screen, J.A. Insignificant Effect of Arctic Amplification on the Amplitude of Midlatitude Atmospheric Waves. *Sci. Adv.* **2020**, *6*, eaay2880. https://doi.org/10.1126/sciadv.aay2880.
151. Tian, F.; Fensholt, R.; Verbesselt, J.; Grogan, K.; Horion, S.; Wang, Y. Evaluating Temporal Consistency of Long-Term Global NDVI Datasets for Trend Analysis. *Remote Sens. Environ.* **2015**, *163*, 326–340. https://doi.org/10.1016/j.rse.2015.03.031.
152. Metcalfe, D.B.; Hermans, T.D.G.; Ahlstrand, J.; Becker, M.; Berggren, M.; Björk, R.G.; Björkman, M.P.; Blok, D.; Chaudhary, N.; Chisholm, C.; et al. Patchy Field Sampling Biases Understanding of Climate Change Impacts across the Arctic. *Nat. Ecol. Evol.* **2018**, *2*, 1443–1448. https://doi.org/10.1038/s41559-018-0612-5.
153. Forkel, M.; Carvalhais, N.; Verbesselt, J.; Mahecha, M.; Neigh, C.; Reichstein, M. Trend Change Detection in NDVI Time Series: Effects of Inter-Annual Variability and Methodology. *Remote Sens.* **2013**, *5*, 2113–2144. https://doi.org/10.3390/rs5052113.
154. Dash, J.; Ogutu, B.O. Recent Advances in Space-Borne Optical Remote Sensing Systems for Monitoring Global Terrestrial Ecosystems. *Prog. Phys. Geogr. Earth Environ.* **2016**, *40*, 322–351. https://doi.org/10.1177/0309133316639403.
155. Bartsch, A.; Widhalm, B.; Leibman, M.; Ermokhina, K.; Kumpula, T.; Skarin, A.; Wilcox, E.J.; Jones, B.M.; Frost, G.V.; Höfler, A.; et al. Feasibility of Tundra Vegetation Height Retrieval from Sentinel-1 and Sentinel-2 Data. *Remote Sens. Environ.* **2020**, *237*, 111515. https://doi.org/10.1016/j.rse.2019.111515.
156. Post, E.; Forchhammer, M.C.; Bret-Harte, M.S.; Callaghan, T.V.; Christensen, T.R.; Elberling, B.; Fox, A.D.; Gilg, O.; Hik, D.S.; Hoye, T.T.; et al. Ecological Dynamics Across the Arctic Associated with Recent Climate Change. *Science (80-)* **2009**, *325*, 1355–1358. https://doi.org/10.1126/science.1173113.
157. Frey, K.E.; Comiso, J.C.; Cooper, L.W.; Grebmeier, J.M.; Stock, L.V. Arctic Ocean Primary Productivity: The Response of Marine Algae to Climate Warming and Sea Ice Decline. *Arct. Rep. Card* **2020**. https://doi.org/10.25923/vtdn-2198.
158. Bohlmann, U.M.; Koller, V.F. ESA and the Arctic—The European Space Agency's Contributions to a Sustainable Arctic. *Acta Astronaut.* **2020**, *176*, 33–39. https://doi.org/10.1016/j.actaastro.2020.05.030.
159. Biskaborn, B.K.; Smith, S.L.; Noetzli, J.; Matthes, H.; Vieira, G.; Streletskiy, D.A.; Schoeneich, P.; Romanovsky, V.E.; Lewkowicz, A.G.; Abramov, A.; et al. Permafrost Is Warming at a Global Scale. *Nat. Commun.* **2019**, *10*, 264. https://doi.org/10.1038/s41467-018-08240-4.
160. Jorgenson, M.T.; Grosse, G. Remote Sensing of Landscape Change in Permafrost Regions. *Permafr. Periglac. Process.* **2016**, *27*, 324–338. https://doi.org/10.1002/ppp.1914.
161. Stow, D.A.; Hope, A.; McGuire, D.; Verbyla, D.; Gamon, J.; Huemmrich, F.; Houston, S.; Racine, C.; Sturm, M.; Tape, K.; et al. Remote Sensing of Vegetation and Land-Cover Change in Arctic Tundra Ecosystems. *Remote Sens. Environ.* **2004**, *89*, 281–308. https://doi.org/10.1016/j.rse.2003.10.018.
162. Smith, L.C.; Sheng, Y.; MacDonald, G.M.; Hinzman, L.D. Disappearing Arctic Lakes. *Science (80-)* **2005**, *308*, 1429–1429. https://doi.org/10.1126/science.1108142.
163. Riseborough, D.; Shiklomanov, N.; Etzelmuller, B.; Gruber, S.; Marchenko, S. Recent Advances in Permafrost Modelling. *Permafr. Periglac. Process.* **2008**, *19*, 137–156. https://doi.org/10.1002/ppp.615.
164. Marchand, N.; Royer, A.; Krinner, G.; Roy, A.; Langlois, A.; Vargel, C. Snow-Covered Soil Temperature Retrieval in Canadian Arctic Permafrost Areas, Using a Land Surface Scheme Informed with Satellite Remote Sensing Data. *Remote Sens.* **2018**, *10*, 1703. https://doi.org/10.3390/rs10111703.
165. Du, J.; Watts, J.D.; Jiang, L.; Lu, H.; Cheng, X.; Duguay, C.; Farina, M.; Qiu, Y.; Kim, Y.; Kimball, J.S.; et al. Remote Sensing of Environmental Changes in Cold Regions: Methods, Achievements and Challenges. *Remote Sens.* **2019**, *11*, 1952. https://doi.org/10.3390/rs11161952.
166. Kumpula, T.; Pajunen, A.; Kaarlejärvi, E.; Forbes, B.C.; Stammler, F. Land Use and Land Cover Change in Arctic Russia: Ecological and Social Implications of Industrial Development. *Glob. Environ. Chang.* **2011**, *21*, 550–562. https://doi.org/10.1016/j.gloenvcha.2010.12.010.
167. Sizov, O.S.; Tsymbarovich, P.R.; Ezhova, E.V.; Soromotin, A.V.; Prikhodko, N.V. Assessment of the Post-Pyrogenic Dynamics of Tundra Vegetation in the Northern Part of Western Siberia over the Past 50 Years (1968–2018) Based on Detailed and High Resolution Remote Sensing Data. *Sovrem. Probl. distantsionnogo Zo. Zemli iz kosmosa* **2020**, *17*, 137–153. https://doi.org/10.21046/2070-7401-2020-17-4-137-153.

168. Esau, I.; Miles, V.V.; Davy, R.; Miles, M.W.; Kurchatova, A. Trends in Normalized Difference Vegetation Index (NDVI) Associated with Urban Development in Northern West Siberia. *Atmos. Chem. Phys.* **2016**, *16*, 9563–9577. https://doi.org/10.5194/acp-16-9563-2016.
169. Vaguet, Y.; Ourng, C.; Moriconi-Ebrard, F. Is the Arctic Really a Frontier? Settlement Dynamics within Various Arctic Limits Based on the Arcticapolis Geohistorical Database. *Espac. Popul. Sociétés* **2021**, 1, https://doi.org/10.4000/eps.10277.
170. Yu, Q.; Epstein, H.E.; Engstrom, R.; Shiklomanov, N.; Strelestskiy, D. Land Cover and Land Use Changes in the Oil and Gas Regions of Northwestern Siberia under Changing Climatic Conditions. *Environ. Res. Lett.* **2015**, *10*, 124020. https://doi.org/10.1088/1748-9326/10/12/124020.
171. Melnikov, V.P.; Osipov, V.I.; Brouchkov, A.V.; Falaleeva, A.A.; Badina, S.V.; Zheleznyak, M.N.; Sadurtdinov, M.R.; Ostrakov, N.A.; Drozdov, D.S.; Osokin, A.B.; et al. Climate Warming and Permafrost Thaw in the Russian Arctic: Potential Economic Impacts on Public Infrastructure by 2050. *Nat. Hazards* **2022**, *112*, 231–251. https://doi.org/10.1007/s11069-021-05179-6.
172. Ramage, J.; Jungsberg, L.; Wang, S.; Westermann, S.; Lantuit, H.; Heleniak, T. Population Living on Permafrost in the Arctic. *Popul. Environ.* **2021**, *43*, 22–38. https://doi.org/10.1007/s11111-020-00370-6.
173. Nyland, K.E.; Gunn, G.E.; Shiklomanov, N.I.; Engstrom, R.N.; Streletskiy, D.A. Land Cover Change in the Lower Yenisei River Using Dense Stacking of Landsat Imagery in Google Earth Engine. *Remote Sens.* **2018**, *10*, 1226. https://doi.org/10.3390/rs10081226.
174. Miller, G.H.; Alley, R.B.; Brigham-Grette, J.; Fitzpatrick, J.J.; Polyak, L.; Serreze, M.C.; White, J.W.C. Arctic Amplification: Can the Past Constrain the Future? *Quat. Sci. Rev.* **2010**, *29*, 1779–1790. https://doi.org/10.1016/j.quascirev.2010.02.008.
175. Andrews, T.; Gregory, J.M.; Webb, M.J. The Dependence of Radiative Forcing and Feedback on Evolving Patterns of Surface Temperature Change in Climate Models. *J. Clim.* **2015**, *28*, 1630–1648. https://doi.org/10.1175/JCLI-D-14-00545.1.
176. Alexeev, V.A.; Langen, P.L.; Bates, J.R. Polar Amplification of Surface Warming on an Aquaplanet in "Ghost Forcing" Experiments without Sea Ice Feedbacks. *Clim. Dyn.* **2005**, *24*, 655–666. https://doi.org/10.1007/s00382-005-0018-3.
177. Haine, T.W.N.; Martin, T. The Arctic-Subarctic Sea Ice System Is Entering a Seasonal Regime: Implications for Future Arctic Amplification. *Sci. Rep.* **2017**, *7*, 4618. https://doi.org/10.1038/s41598-017-04573-0.
178. Graff, L.S.; Iversen, T.; Bethke, I.; Debernard, J.B.; Seland, Ø.; Bentsen, M.; Kirkevåg, A.; Li, C.; Olivié, D.J.L. Arctic Amplification under Global Warming of 1.5 and 2 °C in NorESM1-Happi. *Earth Syst. Dyn.* **2019**, *10*, 569–598. https://doi.org/10.5194/esd-10-569-2019.
179. Virapongse, A.; Pearlman, F.; Pearlman, J.; Murambadoro, M.D.; Kuwayama, Y.; Glasscoe, M.T. Ten Rules to Increase the Societal Value of Earth Observations. *Earth Sci. Inform.* **2020**, *13*, 233–247. https://doi.org/10.1007/s12145-020-00453-w.
180. Plummer, S.; Lecomte, P.; Doherty, M. The ESA Climate Change Initiative (CCI): A European Contribution to the Generation of the Global Climate Observing System. *Remote Sens. Environ.* **2017**, *203*, 2–8. https://doi.org/10.1016/j.rse.2017.07.014.